J. Fluid Mech. (2010), *vol.* 653, *pp.* 99–136.
doi:10.1017/S0022112010000170

Segregation of particles in incompressible random flows: singularities, intermittency and random uncorrelated motion

RUTGER H. A. IJZERMANS†, ELENA MENEGUZ AND MICHAEL W. REEKS

School of Mechanical and Systems Engineering, Newcastle University, Stephenson Building, Claremont Road, Newcastle-upon-Tyne NE1 7RU, UK

(Received 16 June 2008; revised 9 January 2010; accepted 10 January 2010; first published online 13 April 2010)

The results presented here are part of a long-term study in which we analyse the segregation of inertial particles in turbulent flows using the so called full Lagrangian method (FLM) to evaluate the 'compressibility' of the particle phase along a particle trajectory. In the present work, particles are advected by Stokes drag in a random flow field consisting of counter-rotating vortices and in a flow field composed of 200 random Fourier modes. Both flows are incompressible and, like turbulence, have structure and a distribution of scales with finite lifetime. The compressibility is obtained by first calculating the deformation tensor J_{ij} associated with an infinitesimally small volume of particles following the trajectory of an individual particle. The fraction of the initial volume occupied by the particles centred around a position $\boldsymbol{x}$ at time t is denoted by $|J|$, where $J \equiv \det(J_{ij})$ and $J_{ij} \equiv \partial x_i(\boldsymbol{x}_0, t)/\partial x_{0,j}$, $\boldsymbol{x}_0$ denoting the initial position of the particle. The quantity $\mathrm{d}\langle \ln|J|\rangle/\mathrm{d}t$ is shown to be equal to the particle averaged compressibility of the particle velocity field $\langle \nabla \cdot \boldsymbol{v} \rangle$, which gives a measure of the rate-of-change of the total volume occupied by the particle phase as a continuum. In both flow fields the compressibility of the particle velocity field is shown to decrease continuously if the Stokes number St (the dimensionless particle relaxation time) is below a threshold value St_{cr}, indicating that the segregation of particles continues indefinitely. We show analytically and numerically that the long-time limit of $\langle \nabla \cdot \boldsymbol{v} \rangle$ for sufficiently small values of St is proportional to St^2 in the flow field composed of random Fourier modes, and to St in the flow field consisting of counter-rotating vortices. If $St > St_{cr}$, however, the particles are 'mixed'. The level of mixing can be quantified by the degree of random uncorrelated motion (RUM) of particles which is a measure of the decorrelation of the velocities of two nearby particles. RUM is zero for fluid particles and increases rapidly with the Stokes number if $St > St_{cr}$, approaching unity for $St \gg 1$. The spatial averages of the higher-order moments of the particle number density are shown to diverge with time indicating that the spatial distribution of particles may be very intermittent, being associated with non-zero values of RUM and the occurrence of singularities in the particle velocity field. Our results are consistent with previous observations of the radial distribution function in Chun *et al.* (*J. Fluid Mech.*, vol. 536, 2005, p. 219).

† Present address: Royal Dutch Shell plc, Shell Technology Centre Amsterdam, Grasweg 31, 1031 HW Amsterdam, The Netherlands. Email address for correspondence: rutger.ijzermans@shell.com

1. Introduction

Turbulent structures play a crucial role in many particle/fluid processes in the environment and industry: examples include combustion, the production of powder, the motion of droplets in gas/liquid separators and the formation and growth of PM10 particulates in the atmosphere. An area of much investigation is the mechanism for warm-rain initiation and, in particular, the way droplet interactions with the small scales of turbulence in clouds influence the droplet size distribution (Shaw 2003).

It is by now well known that turbulence, contrary to traditionally held views, can demix a suspension of particles (see e.g. Fessler, Kulick & Eaton 1994). The process of segregation depends upon the ratio of the particle response time to the time scale of the turbulent structures in the flow (i.e the Stokes number). Early experiments and simulations (e.g. Crowe, Chung & Troutt 1993) have shown that the demixing reaches a maximum when the particle response time is approximately equal to the time scale of the turbulent structure (i.e the Stokes number ~ 1), the suspended particles being observed to segregate into regions of high strain rate in between the regions of vorticity. In addition Maxey and his co-workers (Maxey 1987; Wang & Maxey 1993) showed that the gravitational settling of particles in homogeneous turbulence was enhanced due to preferential sweeping in the direction of gravity as particles interweave through turbulent structures in the flow. Since then there have been numerous studies to understand and quantify this segregation process. Of particular note have been the seminal studies by Sundaram & Collins (1997) and Wang, Wexler & Zhou (1998) to quantify the influence of segregation on two-particle dispersion and the process of particle agglomeration.

Intrinsically related to the motion of inertial particles is the presence of random uncorrelated motion (RUM) in flow fields that are spatially random but smoothly varying. RUM refers to the possibility that particle trajectories may cross, and relates to the sling effect (see e.g. Falkovich, Fouxon & Stepanov 2002 and Zaichik & Alipchenkov 2003) and to the occurrence of caustics in the particle motion (see Wilkinson *et al.* 2007). Février, Simonin & Squires (2005) have observed that the spatial velocity field resulting from the motion of suspended particles in a direct numerical simulation (DNS) of homogeneous isotropic turbulence consists of two components: a smoothly (continuous) velocity field that accounts for all particle–particle and fluid–particle two point spatial correlations (they referred to this component as the mesoscopic Eulerian particle velocity field (MEPVF)); and a component of spatially random uncorrelated motion which we will refer to here as RUM (the component of RUM) whose contribution to the particle kinetic energy increases as the particle inertia increases. Février *et al.* (2005) attribute this feature to the ability of the particles with inertia to retain the memory of their interaction with very distant, and statistically independent eddies in the flow field.

Segregation and RUM are related to the occurrence of inter-particle collisions as follows (Sundaram & Collins 1997; Wang *et al.* 1998): (i) segregation enhances the particle concentration of certain regions of the flow, (ii) RUM, i.e. the decorrelation of velocity between particles, causes two nearby particles to collide and possibly to coagulate. Segregation is well known to manifest itself especially for $St \sim 1$, whereas the effect of RUM is almost invisible for small particles and becomes increasingly important for larger St. Since the interplay between these two effects determines the collision rate in a turbulent flow, it is essential to quantify segregation and RUM as accurately as possible as a function of the Stokes number and some typical flow properties in order to correctly predict the rate of inter-particle collisions.

In recent years, the process of segregation of inertial particles has been studied from different viewpoints when the Stokes number is relatively small. On the one hand, Chen, Goto & Vassilicos (2006) demonstrated a strong correlation between the positions of small inertial particles and the locations of zero-acceleration points in the carrier flow. On the other hand, Balkovsky, Falkovich & Fouxon (2001) carried out a theoretical analysis based on the assumption that the velocity of inertial particles can be directly related to the carrier flow velocity. By doing so, they were able to show that the segregation of particles continues indefinitely in the course of time, and they showed that the concentration of inertial particles in a turbulent flow is highly intermittent, so the particles are distributed far from uniformly over space. A similar approach was chosen by Chun *et al.* (2005) who demonstrated that the time-converged solution of the radial distribution function is of the form $g(r) \sim r^{\beta}$, where the negative number β is proportional to St^2. In addition, they confirmed this by showing results from a DNS of statistically stationary homogeneous isotropic turbulence.

The understanding of dilute suspensions of inertial particles has been vastly extended by interpreting the motion of particles in terms of dynamical systems theory. The first approach in this direction was given by Sommerer & Ott (1993), and was later specifically applied to the motion of inertial particles in turbulent flows by Bec (2005) and Wilkinson *et al.* (2007). Wilkinson *et al.* (2007) derived an analytical expression for the Lyapunov exponents associated with the motion of inertial particles in physical space. The derivation was based on the assumption that the typical correlation time of the carrier flow was very small, i.e. the Kubo number, $Ku \ll 1$. Unfortunately, this assumption is not exactly valid in real turbulence where $Ku = O(1)$, as Wilkinson *et al.* (2007) acknowledge themselves. Bec (2005) showed that if the particle clustering is fractal, the exponent in the radial distribution function is equal to $\beta = n_d - D_{corr}$, where D_{corr} is the correlation dimension introduced by Hentschel & Procaccia (1983), and n_d is the number of dimensions of the problem ($n_d = 2$ in a two-dimensional flow and $n_d = 3$ in a three-dimensional flow). Bec (2005) expressed the clustering of particles in terms of its fractal dimension in phase space and showed how this was related to the Lyapunov exponents of the $2n_d$-dimensional dynamical system. Bec *et al.* (2007) obtained a correlation dimension D_{corr} by calculating the Lyapunov exponents in a DNS of turbulence for a wide range of Stokes numbers, and found that $n_d - D_{corr}$ scales with St^2, in agreement with the aforementioned results by Chun *et al.* (2005).

In the present paper we employ the full Lagrangian method (FLM) to investigate the segregation and preferential concentration of inertial particles in turbulence-like flows. This method, originally introduced by Osiptsov (2000) but later also used by Reeks (2004) and Healy & Young (2005), consists of calculating the size of an infinitesimally small volume occupied by a group of particles, along the trajectory of one single particle. This immediately yields the concentration of particles along the trajectory, since the inverse of the volume occupied by a fixed number of particles corresponds to the particle concentration by definition. We show how the results from the FLM can be translated into statistics of the particle number density, thus providing a wealth of information on the segregation process. An important advantage of the FLM is that it provides meaningful results for the compressibility along the trajectory of a single particle in the course of time; Lyapunov exponents are, in contrast, only defined in the limit of time approaching infinity (Ott 1994).

We describe for the first time how the FLM can be used to quantify non-uniformities in the spatial distribution of particles, the singularities in the particle velocity field and the presence of RUM. This is an advancement over previous studies such as

Healy & Young (2005) and Osiptsov (2000) where the FLM was primarily employed to determine the particle concentration at some point in the flow domain. What we show here is that the FLM can be further developed and translated into higher-order statistics of the particle number density. These features, which take place on infinitesimally small scales, can not be identified by traditional box counting methods as they rely on finite box sizes by definition. The numerical results obtained from our simulations are validated with respect to available analytical estimates, and compared to the recent numerical results for the radial distribution function by Chun *et al.* (2005) and to the analytical predictions for the particle number density by Balkovsky *et al.* (2001).

Our methods are closely related to the work by Falkovich & Pumir (2004, 2007) who calculated the particle number density along the trajectory continuing past the singularities by changing the sign of the velocity difference. A difference with our method is that Falkovich and Pumir use a nonlinear equation to determine the evolution in time of the particle number density, whereas our equations are linear. This facilitates the numerical solution in our case and allows for analytical solutions to the equations in certain idealized situations.

In order to illustrate our application of the FLM and to understand some of the important underlying features of particle segregation, we limit ourselves to studying the dispersion of particles in relatively simple random flows which share features of real turbulence. The reason for using kinematic simulations at this stage and not direct numerical simulations of turbulence is that flow fields in a DNS are complicated with many scales of spatial and temporal existence. Whilst DNS has been and will continue to be important in identifying turbulent structures and linking them with particular mechanisms, the drawback is that although DNS represents real turbulence at relatively low Reynolds number, we have no real control over the type of structure present in the flow: in fact, we have to identify the structures rather than control them. Therefore we believe there is a clear need for kinematic simulations of turbulence which can be easily implemented, containing structures which we can control and in turn use to study the influence of structures and scales in real turbulence. Thus, simple random flows can be used to identify single effects which might otherwise go unnoticed in more complex flows, their influence being masked by other scales and other effects. As such we regard this study as an important preliminary to a future study of segregation in DNS turbulence where by comparison the ability to change and control the statistics is significantly reduced.

This paper is organized as follows. In § 2 we present the velocity fields of the carrier flow used in the kinematic simulations. In addition, we introduce the equations of motion for the inertial particles, and for the compressibility of the particle phase. In § 3, the results are presented for the dispersion and segregation of heavy particles in random straining flows. Section 4 is devoted to the motion of inertial particles in a flow field composed of a large number of random Fourier modes. Finally, conclusions and prospects for future studies on more complex flows involving DNS are formulated in § 5.

2. Physical–mathematical model

We study the motion of inertial particles in three different flow fields: (i) a non-isotropic random straining flow, (ii) an isotropic random straining flow and (iii) a flow field composed of random Fourier modes. In § 2.1 we describe the random

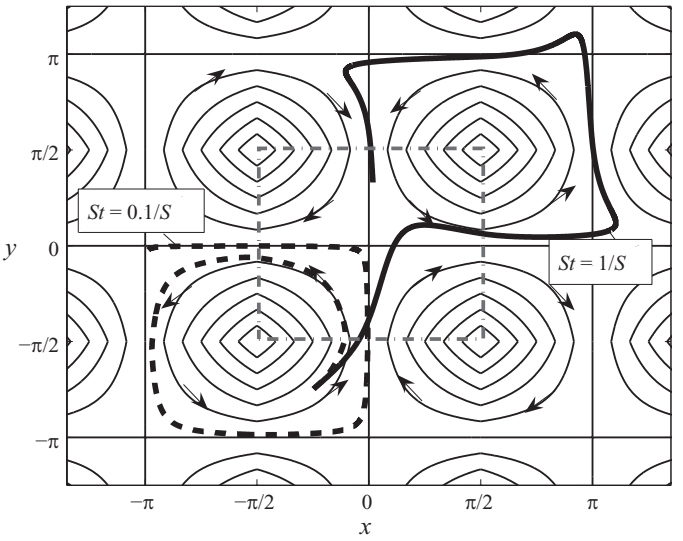

FIGURE 1. Particle trajectories in a frozen field of periodic vortices, for $St = 0.1/S$ (dashed thick line; heavily damped case) and $St = 1/S$ (solid thick line; lightly damped case), where S represents the strain rate in the flow. The two particles are released in $(x, y) = (-\pi/4, -3\pi/4)$ with a velocity equal to the local carrier flow velocity at time $t = 0$, and traced for a time $t = 20$. The highlighted area (dash-dotted line) designates the basic element out of which the entire flow field is constructed.

straining flows, and in § 2.2 we present the flow field composed of random Fourier modes. Finally, the equations of motion for inertial particles are discussed in § 2.3.

2.1. *Description of random straining flows*

2.1.1. *Non-isotropic random straining flow*

We consider a simple two-dimensional homogeneous turbulent flow field composed of pairs of counter-rotating vortices which are periodic in both the x, y directions with the same periodicity. The periodicity is $2\pi k_0^{-1}$, where k_0 is the typical wavenumber of the flow. Here and throughout this paper, we make all variables dimensionless with the wavenumber $k_0[\mathrm{m}^{-1}]$ and a typical velocity scale $u_0[\mathrm{m\,s}^{-1}]$.

Each lattice cell (the basic element, highlighted in figure 1) contains a linear symmetric straining flow field in both the orthogonal directions x and y. A flow field of counter-rotating vortices is constructed from the straining flow in the manner shown in figure 1. The size of the lattice cell, centred around the origin, is $\pi \times \pi$ and the dimensionless strain rate has a value S. The flow field inside the lattice cell is described by the following equations:

$$\left.\begin{aligned} u_x &= Sx, \\ u_y &= -Sy, \end{aligned}\right\} \quad \text{for} \quad x \in [-\pi/2, \pi/2] \quad \text{and} \quad y \in [-\pi/2, \pi/2]. \tag{2.1}$$

The strain rate S is drawn randomly from a uniform distribution $[0, S_0]$, where S_0 is chosen such that the kinetic energy per unit mass of fluid particles (averaged over time and space) is equal to unity (u_0^2 in dimensional form). The spatially averaged kinetic energy at a certain moment in time can be calculated directly from (2.1) as follows:

$$E_{kin,2D} = \frac{1}{\pi^2} \int_{-\pi/2}^{\pi/2} \int_{-\pi/2}^{\pi/2} \frac{1}{2}\left(u_x^2 + u_y^2\right) \mathrm{d}x\, \mathrm{d}y = \frac{\pi^2}{12} S^2. \tag{2.2}$$

The time average of $E_{kin,2D}$ (denoted by the overline with an asterisk) is

$$\overline{E_{kin,2D}}^{*} = \frac{\pi^2}{12}\overline{S^2}^{*} = \frac{\pi^2}{36}S_0^2, \tag{2.3}$$

where we have used that $\overline{S^2}^{*} = S_0^2/3$ if S is randomly drawn from a uniform distribution between 0 and S_0. Thus, we choose the value of S_0 equal to $6/\pi$ so that the mean kinetic energy is equal to unity.

Starting from an initial symmetric straining flow pattern of width π in both the x and y directions, this pattern is repeated front to back in both the x and y directions (see figure 1). We note that each quadrant of this straining flow is a quadrant of one of the counter-rotating vortices formed. The flow velocity u_x in the x direction has a linear saw-tooth profile, with a slope of constant magnitude S but with a change in sign across the vertical centreline of a vortex where the maximum and minimum values of u_x are located. The cellular flow pattern of counter-rotating vortices so formed, persists for a fixed lifetime T_L selected randomly from an exponential distribution with a decay time of T_0; in the present research we take $T_0 = 1$, i.e. $u_0^{-1}k_0^{-1}$ in dimensional form. At the end of the lifetime, a fresh flow field is generated with new values of the T_L and S, and the origin of the pattern at the same time shifted by random displacements Δ_x and Δ_y in both the x and y directions, drawn independently from a uniform distribution $[0, 2\pi]$. This makes the time-averaged flow homogeneous with zero mean in the x and y directions.

Summarizing, the full equations for the flow field are

$$u_x = (-1)^{\gamma_x+\gamma_y}(\hat{x} - \pi\gamma_x)S, \qquad u_y = (-1)^{\gamma_x+\gamma_y+1}(\hat{y} - \pi\gamma_y)S, \tag{2.4}$$

where $\hat{x} \equiv x - \Delta_x$ and $\hat{y} \equiv y - \Delta_y$, and the parameters γ_x and γ_y are defined as

$$\gamma_x \equiv \frac{\hat{x}}{|\hat{x}|}\mathrm{int}\left(\frac{|\hat{x}| + \pi/2}{\pi}\right), \qquad \gamma_y \equiv \frac{\hat{y}}{|\hat{y}|}\mathrm{int}\left(\frac{|\hat{y}| + \pi/2}{\pi}\right). \tag{2.5}$$

In the remainder of this paper, we refer to this flow as 'non-isotropic random straining flow'.

2.1.2. *Isotropic random straining flow with distribution of length scales*

The random straining flow presented in § 2.1.1 is homogeneous but not isotropic, and it contains only one length scale, i.e. the energy spectrum of the flow is a delta function: $E(k) = \delta(k - 1)$. In order to investigate the effect of isotropy and a distribution of length scales on the dispersion and segregation of inertial particles, we modify the flow field by imposing isotropy and by introducing a distribution of scales as follows.

Isotropic flow is created by rotating the flow field described in § 2.1.1 after each time eddy lifetime T_L by a random angle θ, drawn randomly from a uniform distribution between 0 and 2π. At the same time, the flow field is displaced by the orthogonal distances Δ_x and Δ_y, and a different length scale L (i.e. the length scale containing two counter-rotating vortices) of the flow is selected as well. The length scale L is associated with a wavenumber k by the relation $k = 2\pi/L$. The distribution of wavenumbers, and thus of length scales, is chosen in accordance with an energy spectrum proposed by Kraichnan (1970), which is a model for low-Reynolds-number turbulence (Spelt & Biesheuvel 1997); in two dimensions, the energy spectrum is given by

$$E_{2D}(k) = \frac{64}{\sqrt{18\pi}}k^4 \exp(-2k^2). \tag{2.6}$$

Here, the constant $64/\sqrt{18\pi}$ is chosen in such a way that

$$\int_0^\infty E_{2D}(k)\,\mathrm{d}k = 1. \tag{2.7}$$

For a certain length scale L and a strain rate S, the mean kinetic energy per unit mass of fluid particles can be calculated in the same way as was done in (2.2), yielding $\overline{E_{kin,2D}}^* = \overline{(S^2L^2)/48}^*$. We suppose that the mean kinetic energy of fluid particles, which is normalized to unity, is equal for all wavelengths: $(S^2L^2)/48 = 1,\ \forall\ L$. Thus, we choose $S = \sqrt{48}/L = k\sqrt{12}/\pi$. It is noted that the highest velocity gradients occur for the smallest scales, which is qualitatively in accordance with real turbulence (Frisch 1995). The wavelength k is determined randomly from a probability density function (PDF) equal to the right-hand side of (2.6); since each mode contains the same amount of kinetic energy, the prescribed energy spectrum is then automatically satisfied.

Thus, the full equations for the flow field are, as a function of the random variables θ, k, Δ_x and Δ_y:

$$u_\xi = (-1)^{\gamma_\xi+\gamma_\eta} S(\hat{\xi} - \gamma_\xi L/2), \qquad u_\eta = (-1)^{\gamma_\xi+\gamma_\eta+1} S(\hat{\eta} - \gamma_\eta L/2), \tag{2.8}$$

where $S = k\sqrt{12}/\pi$, $L = 2\pi/k$, $\hat{\xi} \equiv \xi - \Delta_x$ and $\hat{\eta} \equiv \eta - \Delta_y$; ξ and η are coordinates in a rotated frame of reference, following from $(\xi, \eta)^T = \boldsymbol{R}(\theta)(x, y)^T$ where $\boldsymbol{R}(\theta)$ is a rotation matrix:

$$\boldsymbol{R}(\theta) = \begin{bmatrix} \cos\theta & \sin\theta \\ -\sin\theta & \cos\theta \end{bmatrix}. \tag{2.9}$$

The parameters γ_ξ and γ_η in (2.8) are defined as

$$\gamma_\xi \equiv \frac{\hat{\xi}}{|\hat{\xi}|}\mathrm{int}\left(\frac{|\hat{\xi}| + L/4}{L/2}\right), \qquad \gamma_\eta \equiv \frac{\hat{\eta}}{|\hat{\eta}|}\mathrm{int}\left(\frac{|\hat{\eta}| + L/4}{L/2}\right). \tag{2.10}$$

The velocity field in the Cartesian non-rotated frame of reference can be obtained from (2.8) by

$$\begin{bmatrix} u_x \\ u_y \end{bmatrix} = \boldsymbol{R}^{-1}(\theta) \begin{bmatrix} u_\xi \\ u_\eta \end{bmatrix}. \tag{2.11}$$

In the remainder of this paper, we refer to this flow as 'isotropic random straining flow'.

2.2. *Flow field composed of random Fourier modes*

As an alternative to the isotropic and non-isotropic random straining flow presented in § 2.1, we simulate a turbulent velocity field in a three-dimensional periodic box by a large number of random Fourier modes, similar to, for example, Reeks (1977), Maxey (1987) and Spelt & Biesheuvel (1997). The modes are chosen in such a way that the associated energy spectrum of the flow field again approximates the form originally proposed by Kraichnan (1970).

The velocity field is represented as a Fourier series of N modes ($N = 200$ in our simulations):

$$\boldsymbol{u}(\boldsymbol{x}, t) = \sum_{n=1}^{N} \left[\frac{\boldsymbol{a}^{(n)} \times \boldsymbol{k}^{(n)}}{|\boldsymbol{k}^{(n)}|} \cos\left(\boldsymbol{k}^{(n)} \cdot \boldsymbol{x} + \omega^{(n)} t\right) + \frac{\boldsymbol{b}^{(n)} \times \boldsymbol{k}^{(n)}}{|\boldsymbol{k}^{(n)}|} \sin\left(\boldsymbol{k}^{(n)} \cdot \boldsymbol{x} + \omega^{(n)} t\right) \right], \tag{2.12}$$

with random coefficients $\boldsymbol{a}^{(n)}$ and $\boldsymbol{b}^{(n)}$, random wavenumbers $\boldsymbol{k}^{(n)}$ and random wave frequencies $\omega^{(n)}$. It is noted that $\nabla\cdot\boldsymbol{u}=0$, i.e. the flow is incompressible. In order to guarantee the periodicity of the flow in a cubed box of dimensions $\mathscr{L}\times\mathscr{L}\times\mathscr{L}$, the wavenumber components $k_i^{(n)}(i=1,2,3)$ are chosen as follows:

$$k_1^{(n)}=\frac{2\pi m_1^{(n)}}{\mathscr{L}},\qquad k_2^{(n)}=\frac{2\pi m_2^{(n)}}{\mathscr{L}},\qquad k_3^{(n)}=\frac{2\pi m_3^{(n)}}{\mathscr{L}};\qquad m_1^{(n)},m_2^{(n)},m_3^{(n)}\in\mathbb{N}. \quad (2.13)$$

In the present study we take $\mathscr{L}=10\mathscr{L}_{11}$, where $\mathscr{L}_{11}=\sqrt{2\pi}$ is the integral length scale of the flow (Spelt & Biesheuvel 1997). The integer numbers $m_1^{(n)}$, $m_2^{(n)}$ and $m_3^{(n)}$ are chosen randomly in such a way that the length $|\boldsymbol{k}^{(n)}|$ is approximately equal to the ideal wavenumber $k_{id}^{(n)}$ which can be determined from the Kraichnan energy spectrum as follows:

$$\int_0^{k_{id}^{(n)}}E_{3D}(k)\,\mathrm{d}k=\int_0^{k_{id}^{(n)}}\frac{3}{2}E_{2D}(k)\,\mathrm{d}k=\frac{3}{2}\frac{(n-1/2)}{N}, \quad (2.14)$$

where $E_{2D}(k)$ is defined in (2.6). A detailed procedure for determining the integer numbers m_1, m_2 and m_3 is given in the Appendix. The maximum of $E_{3D}(k)$ is situated at $k=1$ and the total kinetic energy $\int_0^\infty E_{3D}(k)\,\mathrm{d}k=3/2$ (i.e. $(3/2)u_0^2$ in dimensional form). The use of the Kraichnan energy spectrum results in a relatively small separation of scales; in our simulations, the smallest wavenumber $k^{(1)}\simeq 0.25$ and the largest wavenumber $k^{(N)}\simeq 2.14$. This flow field can be seen as a natural extension of the two-dimensional models consisting of counter-rotating vortices presented in § 2.1, which contain only one single scale at a certain moment in time.

The wave frequencies $\omega^{(n)}$ are selected randomly from a Gaussian distribution with zero mean and a variance of $a^*k^{(n)}$. Following Hunt, Buell & Wray (1987) and Spelt & Biesheuvel (1997), we take $a^*=0.40$. This means that the Kubo number, defined as $Ku\equiv u_0k_0/\tau_f$ with τ_f a typical correlation time of the flow, is approximately equal to $Ku\simeq 1/0.40=2.5$. This value is reasonable in view of fully developed turbulence, in which $Ku=O(1)$ (see Wilkinson *et al.* 2007).

Finally, the coefficients $\boldsymbol{a}^{(n)}$ and $\boldsymbol{b}^{(n)}$ are determined by choosing a random direction in $\mathbb{R}^3$ and by picking a length randomly from a Gaussian distribution with zero mean and a variance $9/2N$. By doing so, the time-averaged kinetic energy at a certain position in the flow, defined as

$$\overline{E_{kin}(\boldsymbol{x})}^*\equiv\frac{1}{T}\lim_{T\to\infty}\int_0^T\frac{1}{2}|\boldsymbol{u}(\boldsymbol{x},t)|^2\,\mathrm{d}t=\frac{1}{2}\sum_{n=1}^{N}\frac{1}{|\boldsymbol{k}^{(n)}|^2}\left[\frac{1}{2}|\boldsymbol{a}^{(n)}\times\boldsymbol{k}^{(n)}|^2+\frac{1}{2}|\boldsymbol{b}^{(n)}\times\boldsymbol{k}^{(n)}|^2\right], \quad (2.15)$$

is approximately equal to $3/2$ for all $\boldsymbol{x}$. In the flow field used in the present study, the time-averaged energy contained in the cosine modes associated with $\boldsymbol{a}^{(n)}$ is lower than the ideal value of $3/4$ by a percentage 3.45 %, whereas the average energy contained in the sine modes associated with $\boldsymbol{b}^{(n)}$ is higher than $3/4$ by a percentage of 3.99 %. These differences are due to the finite number of modes N which results in

$$\sum_{n=1}^{N}\left|\boldsymbol{a}^{(n)}\times\frac{\boldsymbol{k}^{(n)}}{|\boldsymbol{k}^{(n)}|}\right|^2\quad\text{and}\quad\sum_{n=1}^{N}\left|\boldsymbol{b}^{(n)}\times\frac{\boldsymbol{k}^{(n)}}{|\boldsymbol{k}^{(n)}|}\right|^2$$

not being exactly equal to the expected value $(2/3)\sum_{n=1}^{N}(9/2N)$ (the prefactor $2/3$ is a consequence of isotropy).

The present flow does not contain sweeping of small scales by large scales, although this effect has been shown to be important for the instantaneous distribution of inertial particles in turbulent flows (Chen *et al.* 2006). Whilst an attempt has been made to include sweeping in kinematic simulations (Fung *et al.* 1992), the resulting flow field is not perfectly incompressible imposing serious limitations when studying segregation. In this application of FLM we have excluded such features, deferring them to a future DNS application where they can be normally considered without ambiguity.

2.3. *Equations of motion of inertial particles*

We consider small spherical particles with a density ρ_p and a radius a_p immersed in a carrier flow with a density ρ and kinematic viscosity ν. Upon assuming the density of the particle to be much higher than the density of the carrier flow, i.e. $\rho_p/\rho \gg 1$, the equations of motion of each particle can be derived from the expression given in Maxey & Riley (1983):

$$\frac{\mathrm{d}\boldsymbol{x}}{\mathrm{d}t} = \boldsymbol{v}, \qquad \frac{\mathrm{d}\boldsymbol{v}}{\mathrm{d}t} = \frac{1}{St}(\boldsymbol{u} - \boldsymbol{v}), \tag{2.16}$$

where $\boldsymbol{x}$ and $\boldsymbol{v}$ denote the position and the velocity of the particle, respectively, and $\boldsymbol{u} = \boldsymbol{u}(\boldsymbol{x}, t)$ is the velocity of the carrier flow at the position of the particle. All variables have been made dimensionless by a typical wavenumber k_0 and a typical velocity u_0 of the carrier flow. The dimensionless parameter $St \equiv \tau_p u_0 k_0$ denotes the Stokes number, where τ_p denotes the Stokes particle relaxation time defined as $\tau_p \equiv 2a_p^2\rho_p/9\nu\rho$. In this study, gravity is neglected to isolate effects which occur purely due to the finite inertia of particles.

The segregation in the course of time can be analysed by using the FLM (see Osiptsov 2000; Reeks 2004; Healy & Young 2005). For this purpose, we investigate the volume occupied by a large number of particles, which are initially released inside a relatively small volume centred around $\boldsymbol{x}_0$. The deformation of such a volume is characterized by the temporal evolution of the unit deformation tensor J_{ij}, defined by

$$J_{ij} \equiv \frac{\partial x_i(\boldsymbol{x}_0, t)}{\partial x_{0,j}}, \tag{2.17}$$

where $\boldsymbol{x}_0$ is the position of the particle at some initial time, say $t = 0$. Differentiating (2.17) with respect to time gives

$$\frac{\mathrm{d}}{\mathrm{d}t} J_{ij} = \frac{\partial v_i(\boldsymbol{x}_0, t)}{\partial x_{0,j}}. \tag{2.18}$$

The second derivative with respect to time is

$$\frac{\mathrm{d}^2}{\mathrm{d}t^2} J_{ij} = \frac{\partial}{\partial x_{0,j}}\left(\frac{\mathrm{d}v_i(\boldsymbol{x}_0, t)}{\mathrm{d}t}\right) = \frac{1}{St}\left(\frac{\partial x_k}{\partial x_{0,j}}\right)\frac{\partial}{\partial x_k}u_i(\boldsymbol{x}, t) - \frac{1}{St}\frac{\partial v_i(\boldsymbol{x}_0, t)}{\partial x_{0,j}}. \tag{2.19}$$

Inserting (2.17) and (2.18) into (2.19) results in the equations of motion of each component J_{ij}:

$$\frac{\mathrm{d}J_{ij}}{\mathrm{d}t} = \dot{J}_{ij}, \qquad \frac{\mathrm{d}}{\mathrm{d}t}\dot{J}_{ij} = \frac{1}{St}\left(J_{kj}\frac{\partial u_i}{\partial x_k} - \dot{J}_{ij}\right). \tag{2.20}$$

We choose as initial conditions $\boldsymbol{u} = \boldsymbol{v}$, $J_{ij}(0) = \delta_{ij}$ and $\dot{J}_{ij}(0) = \partial u_i(\boldsymbol{x}_0, 0)/\partial x_j$. The total deformation J is equal to the determinant of the tensor J_{ij}: $J = \det(J_{ij})$.

If the initial distribution of particles is uniform over a certain domain, the deformation in the course of time is inversely proportional to the particle number

density n measured along the trajectory of one reference particle:

$$|J(t)| = n^{-1}(t), \tag{2.21}$$

where n is normalized so that it is equal to $|J|^{-1} = 1$ at time $t = 0$. Equation (2.21) implies that $|J|^{\alpha} = n^{-\alpha}$ for any $\alpha \in \mathbb{R}$. The average over all particles, denoted by the brackets '$\langle\ \rangle$', is then

$$\langle |J|^{\alpha} \rangle = \langle n^{-\alpha} \rangle. \tag{2.22}$$

The spatially averaged value of any quantity Φ can be related to the particle averaged value as follows:

$$\langle \Phi \rangle = \frac{1}{\Omega} \int_{\Omega} \Phi(\boldsymbol{x}) n(\boldsymbol{x})\, \mathrm{d}\boldsymbol{x} = \overline{n\Phi}, \tag{2.23}$$

where the overbar ($^{-}$) denotes a spatial average over the domain (of size Ω) considered. Combination of (2.22) and (2.23) yields

$$\overline{n^{\alpha}} = \langle |J|^{1-\alpha} \rangle, \quad \forall \quad \alpha \in \mathbb{R}. \tag{2.24}$$

Thus a spatially averaged moment of the particle number density $\overline{n^{\alpha}}$ can be calculated directly from the deformation J along sufficiently many particle trajectories.

The FLM can also be used to determine the compressibility of the particle phase. Starting again from (2.21), we can write

$$\frac{\mathrm{d}}{\mathrm{d}t} \ln |J| = -\frac{\mathrm{d}}{\mathrm{d}t} \ln n. \tag{2.25}$$

Because $\mathrm{d}n/\mathrm{d}t = -n\nabla \cdot \boldsymbol{v}$, (2.25) can be rewritten as

$$\frac{\mathrm{d}}{\mathrm{d}t} \ln |J| = \nabla \cdot \boldsymbol{v}. \tag{2.26}$$

If the carrier flow is incompressible, $\mathrm{d} \ln |J|/\mathrm{d}t$ is related to the velocity of the carrier fluid at the position of the particle as an expansion in the Stokes number as follows:

$$\frac{\mathrm{d}}{\mathrm{d}t} \ln |J| = \nabla \cdot \boldsymbol{v} = -St\, Q + St^2 \frac{\mathrm{d}Q}{\mathrm{d}t} + O(St^3), \tag{2.27}$$

where we have used the fact that (2.16) can be rewritten as $\boldsymbol{v} = \boldsymbol{u} - St\, \mathrm{D}\boldsymbol{u}/\mathrm{D}t + St^2 \mathrm{d}(\boldsymbol{u} \cdot \nabla \boldsymbol{u})/\mathrm{d}t + O(St^3)$. The parameter Q in (2.27) is defined as

$$Q \equiv \left(\frac{\partial u_i}{\partial x_j} \frac{\partial u_j}{\partial x_i} \right), \tag{2.28}$$

and should be evaluated at the position of the particle. If we take into account only the first-order term in Stokes on the right-hand side of (2.27), we retrieve the following approximation, first proposed by Maxey (1987):

$$\frac{\mathrm{d}}{\mathrm{d}t} \ln |J| = -St\, Q + O(St^2), \tag{2.29}$$

It can be shown that Q is equal to (IJzermans 2007):

$$Q = \alpha_1^2 + \alpha_2^2 + \alpha_3^2, \tag{2.30}$$

where α_1, α_2 and α_3 are the three eigenvalues of the tensor $\partial u_i/\partial x_j$. Due to incompressibility, the eigenvalues can either be all real, or complex of the form $\alpha_1 = \alpha_{\mathrm{Re}} + \mathrm{i}\alpha_{\mathrm{Im}}$, $\alpha_2 = \alpha_{\mathrm{Re}} - \mathrm{i}\alpha_{\mathrm{Im}}$, $\alpha_3 = -2\alpha_{\mathrm{Re}}$. Equations (2.29) and (2.30) show that inertial particles diverge in regions where α_1, α_2, α_3 are complex and $\alpha_{\mathrm{Im}}^2 > 3\alpha_{\mathrm{Re}}^2$; this

is typically the case in regions of high vorticity and relatively low strain; indeed, a region with complex eigenvalues is defined as a vortex region by Chong, Perry & Cantwell (1990). In all other regions, inertial particles with a sufficiently small Stokes number are concentrated. Thus, small heavy particles can agglomerate inside a vortex, provided the local strain is sufficiently high. A striking example is a Burgers vortex, in which small heavy particles do accumulate (Marcu, Meiburg & Newton 1995).

Alternatively, Q can be related to the pressure of the carrier flow field p by taking the divergence of the incompressible Navier–Stokes equation (see e.g. Elperin, Kleeorin & Rogashevskii 1996):

$$Q = \nabla \cdot (\boldsymbol{u} \cdot \nabla \boldsymbol{u}) = -\frac{1}{\rho}\nabla^2 p, \tag{2.31}$$

where we have used that $\nabla \cdot \boldsymbol{u} = 0$ in order to eliminate the time derivative of $\boldsymbol{u}$ and the viscosity term in the Navier–Stokes equation. This conclusion is corroborated by the numerical experiments by Luo, Fan & Cen (2007), who found a good correlation between the $\nabla^2 p$ field and the concentration of inertial particles obtained from direct numerical simulations in incompressible free shear flows.

A method similar to the FLM was proposed by Falkovich and Pumir, first for infinitesimally small St (Falkovich & Pumir 2004) and subsequently for any St (Falkovich & Pumir 2007). In both studies, Falkovich and Pumir used a nonlinear equation for the time evolution of the deformation tensor.

3. Dispersion and segregation of particles in random straining flow

In this section, we present results for the dispersion of inertial particles in the random straining flows introduced in § 2.1. By means of an introduction and in order to show some basic features of the motion of inertial particles inside this type of flow, we briefly discuss some results for the case where the flow field is frozen, i.e. the flow field is given by (2.4) with $\Delta_x = 0$ and $\Delta_y = 0$ for all time.

Based on Stokes drag (see (2.16)), the particle equation of motion within a straining region, with constant strain rate S, is

$$\ddot{x} + St^{-1}\dot{x} + St^{-1}Sx = 0, \qquad \ddot{y} + St^{-1}\dot{y} - St^{-1}Sy = 0, \tag{3.1}$$

where x and y are measured from a stagnation point. We note that the equations in (3.1) are those of a damped simple harmonic oscillator and as a consequence there are two types of motion, namely heavily damped for $St < 0.25/S$ and lightly damped for $St > 0.25/S$. This has some bearing on the motion of the particle within these vortices. For heavily damped motion, a particle remains trapped within a vortex but approaches the extremity (the stagnation region) in a manner which decreases exponentially with time. On the other hand, for lightly damped motion the particle can escape the vortex and in doing so, overshoot into an adjacent vortex. This has been referred to as the 'sling-shot' effect (Falkovich *et al.* 2002) and it is this type of motion that gives rise to RUM. Both types of behaviour are illustrated in figure 1 for particle response times $St = 0.1/S$ (heavily damped) and $St = 1/S$ (lightly damped), respectively.

The equations of motion for J_{ij}, given in (2.20), can be expressed as follows if a particle is inside a straining region with constant strain rate S:

$$\ddot{J}_{11} + St^{-1}\dot{J}_{11} + St^{-1}SJ_{11} = 0, \qquad \ddot{J}_{22} + St^{-1}\dot{J}_{22} - St^{-1}SJ_{22} = 0. \tag{3.2}$$

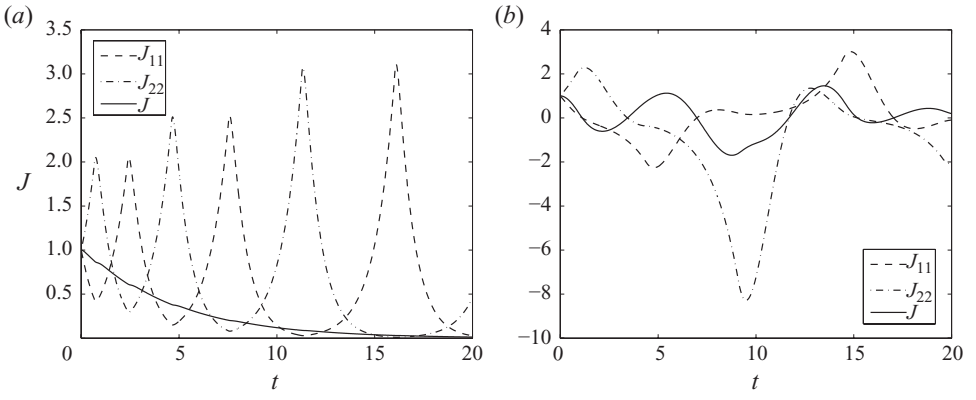

FIGURE 2. Values of the deformation J and the components of the deformation matrix J_{11} and J_{22} in the frozen field of periodic vortices depicted in figure 1, for (a) the heavily damped case $St = 0.1/S$, and (b) the lightly damped case $St = 1/S$. The values of J_{11}, J_{22} and J are calculated along the same two particle trajectories as plotted in figure 1. The strain rate is taken as $S = \sqrt{\overline{S^2}^*} = \sqrt{12}/\pi$.

Since both expressions in (3.2) are linear, J_{11} and J_{22} can be solved analytically:

$$\left.\begin{aligned} J_{11} &= a_{11}\exp\big(\lambda_1^+(t-t')\big) + a_{12}\exp\big(\lambda_2^+(t-t')\big), \\ J_{22} &= a_{21}\exp\big(\lambda_1^-(t-t')\big) + a_{22}\exp\big(\lambda_2^-(t-t')\big), \end{aligned}\right\} \tag{3.3}$$

where t' denotes the time at which the particle enters the straining region, and $\lambda_i^{\pm}$ is

$$\lambda_1^{\pm} = \frac{1}{2St}\big(-1 + \sqrt{1 \pm 4St\,S}\big), \qquad \lambda_2^{\pm} = \frac{1}{2St}\big(-1 - \sqrt{1 \pm 4St\,S}\big). \tag{3.4}$$

The coefficients a_{ij} in (3.3) depend upon the values of J_{ij} and $\dot{J}_{ij}$ when the particle enters the straining region:

$$\left.\begin{aligned} a_{11} &= \frac{\dot{J}_{11}(t') - \lambda_1^+ J_{11}(t')}{\lambda_1^+ - \lambda_2^+}, \qquad a_{12} = \frac{\dot{J}_{11}(t') - \lambda_2^+ J_{11}(t')}{\lambda_2^+ - \lambda_1^+}, \\ a_{21} &= \frac{\dot{J}_{22}(t') - \lambda_1^+ J_{22}(t')}{\lambda_1^- - \lambda_2^-}, \qquad a_{22} = \frac{\dot{J}_{22}(t') - \lambda_2^- J_{22}(t')}{\lambda_2^- - \lambda_1^-}. \end{aligned}\right\} \tag{3.5}$$

Note that in this linear system the equations of motion of J_{11} and J_{22} are the same as those of x and y and that the components of J_{ij} are dependent on the position of the particle only through the time at which the strain rate experienced by the particle changes sign.

Figures 2(a) and 2(b) show the corresponding values of $J(t)$ along the heavily damped and lightly damped particle trajectories plotted in figure 1. In both cases the value of J approaches zero as $t \to \infty$. However in the lightly damped case $J(t)$ passes through zero at intermediate times as the particle oscillates backwards and forwards across a stagnation line. In so doing the value of J oscillates from positive to negative, with the corresponding elemental volume rotating through 180° as it passes through zero volume. Each time $J(t)$ passes through zero, the corresponding particle concentration becomes infinite instantaneously. This raises the possibility that such events may occur in real turbulent flows and that the process of particle dispersion could be a highly intermittent process associated with large deviations in the particle concentrations (see also Healy & Young 2005). It also indicates the conditions under which particle trajectories cross and RUM becomes important.

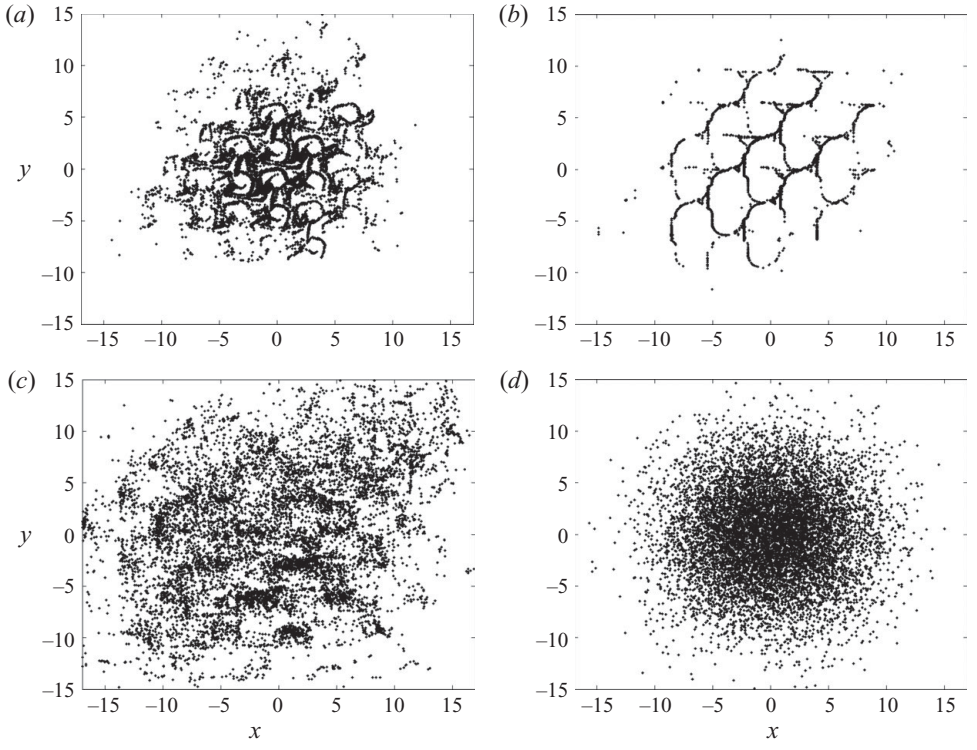

FIGURE 3. (*a–c*) Positions of 10^4 particles after time $t = 20$ in a non-isotropic random straining flow, for $St = 0.05$ (*a*), $St = 0.5$ (*b*) and $St = 5$ (*c*). (*d*) Position of one single particle after $t = 20$ in 10^4 separate realizations of the non-isotropic random straining flow, for $St = 0.5$.

3.1. *Particle dispersion in non-isotropic random straining flow*

Figure 3(*a–c*) shows the positions of 10^4 particles after 20 dimensionless time steps from their release into one single realization of the flow. Each particle was released at a randomly selected position inside a box of size $2\pi \times 2\pi$ centred around the origin, with an initial velocity equal to the local carrier flow velocity. The cases in figure 3(*a–c*) refer to particles with Stokes numbers of $St = 0.05$, $St = 0.5$ and $St = 5$, respectively. Although the particles are non-uniformly distributed in all three cases, the segregation of particles is most marked for the case of $St = 0.5$. The role of particle response time here determines the degree to which particles can segregate into the stagnation regions of the flow pattern as the flow field is shifted in position from one eddy lifetime to the next. Evidently, this mechanism is most effective for the case of $St = 0.5$, but in all cases (even with $St = 0.5$) the segregation does not align with the location of the stagnation lines at any instant of time. Even so the pattern of segregation gets stringier as time progresses, the rate at which that happens being greatest for $St \sim 0.5$.

In contrast, figure 3(*d*) shows the final position of one single particle with $St = 0.5$ released with the same distribution of initial velocities as in the previous cases, in 10^4 separate realizations of the flow. In this case there is no evidence of segregation – the result being the superposition of all the concentration patterns in figure 3(*b*) uniformly shifted over a lattice spacing.

Based on the particle positions shown in figure 3(*d*), it is possible to determine the diffusion coefficient of inertial particles. By repeating the simulation for a wide range

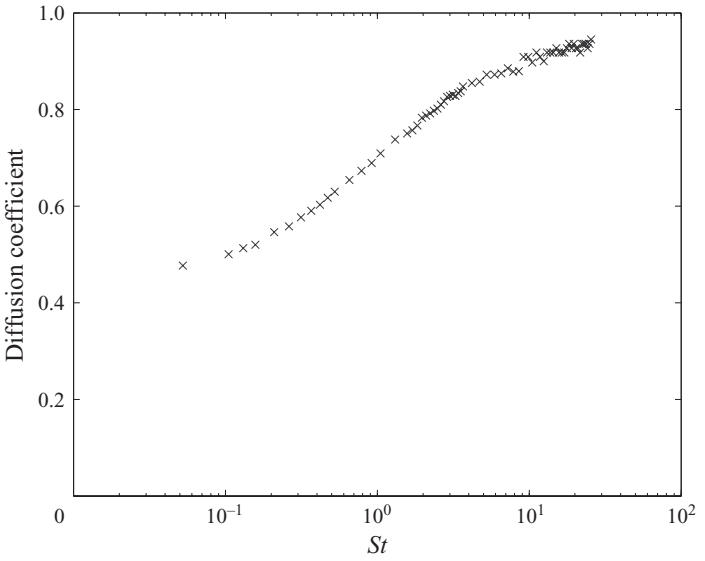

FIGURE 4. Long-time particle diffusion coefficient in the non-isotropic random straining flow, as a function of the Stokes number.

of values of the Stokes number, one arrives at the diffusion coefficient as a function of St. Figure 4 shows the long-term values of the particle diffusion coefficient as a function of the Stokes number, obtained by repeating the simulation of 10^3 particles in 10^3 realizations of the non-isotropic random straining flow for many different Stokes numbers. The long-term values exhibit no intermediate peaking of the particle diffusion coefficient as with the particle segregation: the particle diffusion coefficient increases with increasing particle response time reaching an asymptotic limit for very large response times which is approximately twice as large as that of the fluid particle (i.e. a passive scalar). This latter result is consistent with an early analysis (Reeks 1977) and with results from the simulation of particles in a DNS of homogeneous isotropic turbulence (Squires & Eaton 1991). The value of the diffusion coefficient in the large particle limit $St \gg 1$ can be estimated from the mean kinetic energy of the particles at $t = 0$ and the mean eddy lifetime: $\overline{E_{kin,2D}}^{*} \times \overline{T_L}^{*} = 1$. Evidently, this result is in very good agreement with the numerically obtained value for large St plotted in figure 4.

3.2. *Statistics of the compressibility of the particle phase*

Now that we have given a few illustrations of particle segregation in random straining flows and how it depends on the Stokes number, we quantify the deformation of the particle phase in terms of the deformation tensor J_{ij} defined in (2.20).

In figure 5 we plot the values of $t^{-1} \ln |J|$ for two particle response times, i.e. $St = 0.1$ and $St = 1$. This quantity may be interpreted as the compressibility of the particle phase because

$$\lim_{t\to\infty} t^{-1} \ln |J| = \lim_{t\to\infty} \mathrm{d}(\ln |J|)/\mathrm{d}t = \lim_{t\to\infty} \nabla \cdot \boldsymbol{v}, \tag{3.6}$$

where $\nabla \cdot \boldsymbol{v} = \nabla \cdot \boldsymbol{v}(\boldsymbol{x}_0, t)$ in material coordinates along the Lagrangian trajectory of the particle. The result of figure 5 is obtained by calculating J along one single particle trajectory in one single realization of the flow. Apparently, the rate-of-compression $t^{-1} \ln |J|$ quickly approaches a negative value if $St = 0.1$, the small fluctuations being

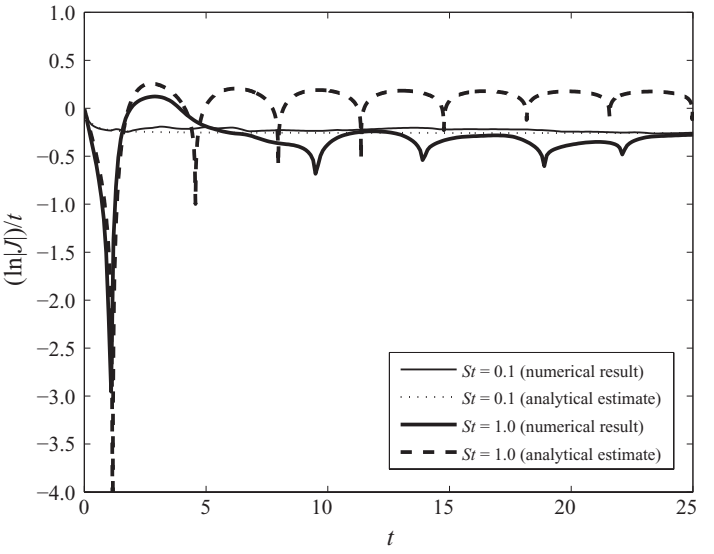

FIGURE 5. Rate-of-compression as a function of time, calculated along an individual particle trajectory for $St = 0.1$ and $St = 1$ in the non-isotropic random straining flow. The results are compared with analytical estimates obtained from (3.3) with $S = \sqrt{\overline{S^2}^*} = \sqrt{12}/\pi$.

a result of the discontinuities in the strain rate S and in the displacements Δ_x and Δ_y, which are reselected after every eddy lifetime T_L. For the case $St = 1$, the value of $t^{-1} \ln |J|$ in the course of time is marked by intermittent negative peaks. These peaks occur when J becomes equal to zero. For both Stokes numbers, the long-term value of $t^{-1} \ln |J|$ approaches a negative constant, indicating that the segregation process continues indefinitely in the course of time.

For the sake of comparison, figure 5 also shows an analytical expression for $t^{-1} \ln |J|$ in the course of time, obtained from the solutions presented in (3.3) and $J = J_{11} J_{22}$. It is noted that this solution is exact if $\Delta_x = 0$ and $\Delta_y = 0$ and if the straining region is stretching to infinity ($x \to \pm\infty$, $y \to \pm\infty$) without discontinuities. Although clearly these conditions are not met in the non-isotropic straining flow, the analytical estimate for $St = 0.1$ is very much in accordance with the numerically obtained result: the long-time values obtained from the numerical simulation and the analytical estimate are hardly distinguishable from each other. Alternatively, the long-term value of $t^{-1} \ln |J|$ in the limit of a vanishing Stokes number can be determined from (2.29); using the fact that the value of $Q = 2S^2$ everywhere in the flow at a certain moment in time, we arrive at $\lim_{t\to\infty} t^{-1} \ln |J| \simeq -2St\, \overline{S^2}^* = -2St\, S_0^2/3 = -2 \times 0.1 \times (12/\pi^2) \simeq -0.243$, which is in good agreement with the numerically determined long-time value for $St = 0.1$ in figure 5. For $St = 1$ on the other hand, we see that the analytical expression is qualitatively in agreement with the numerical result, especially for $t < 5$. For longer times, however, the analytical expression goes to a positive value of $t^{-1} \ln |J|$, whereas the numerical simulation yields a negative value of $t^{-1} \ln |J|$ as $t \to \infty$. Nevertheless, the frequency of the intermittent negative peaks, which are caused by J being equal to zero, is relatively well predicted.

Physically, the value of $J = 0$ means that the particle concentration becomes infinite instantaneously and that trajectories of two particles may cross. Therefore the frequency at which J passes through zero, $\omega_{J=0}$, can be an important parameter

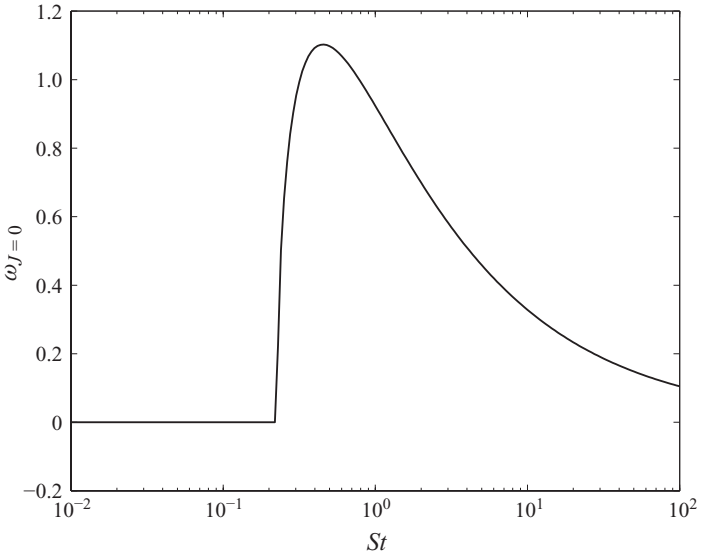

FIGURE 6. The frequency at which the deformation J passes through zero, $\omega_{J=0}$, given by the analytical expression in (3.7), as a function of the Stokes number. The strain rate is taken as $S = \sqrt{12}/\pi$.

characterizing the spatial intermittency in the distribution of particles. It is possible to estimate $\omega_{J=0}$ from the analytical expression of the evolution of J in the course of time, presented in (3.3). This frequency is equal to the imaginary part of the complex eigenvalues given in (3.4):

$$\omega_{J=0} = \frac{1}{2St}\sqrt{4StS - 1}. \tag{3.7}$$

The result is given in figure 6, for a value of the strain rate $S = \sqrt{\overline{S^2}^*} = \sqrt{12}/\pi$. If $St < 0.25/S$, $\omega_{J=0} = 0$ and J never passes through zero, due to the fact that all eigenvalues in (3.4) are real. If $St > 0.25/S$, however, $\omega_{J=0}$ increases very rapidly with St and reaches a maximum at $St = 0.5/S$. Thus, the phenomenon of two particles at the same position with different velocities (caustics) is apparently completely absent for small Stokes numbers and increases rapidly as the Stokes number goes beyond a threshold value of $0.25/S$. These results are in correspondence with the observation of Wilkinson *et al.* (2007), who show that in real turbulence the collision rate (i.e. the probability that particle trajectories cross) has an activation dependence on the Stokes number.

The intermittency in the graph of $t^{-1}\ln|J|$ is not visible if the rate-of-compression is calculated over one particle in a large number of different realizations of the carrier flow. This is mainly due to the fact that the peaks are situated at different instants in time in different realizations, thus yielding a smooth curve for $t^{-1}\langle\ln|J|\rangle$. The rate-of-compression averaged over one single inertial particle in 10^5 separate realizations of the flow field, $t^{-1}\langle\ln|J|\rangle$, is shown in figure 7 for four different values of the Stokes number. In the cases of $St = 0.1$, 0.5 and 1, the compressibility reaches a constant negative value consistent with a continuous compression of the particle phase in the long term. The maximum value of the averaged rate-of-compression in these three cases is for $St = 0.5$, which is in agreement with the results shown in figure 3(*a–c*). The implication of the constant negative value of the compressibility

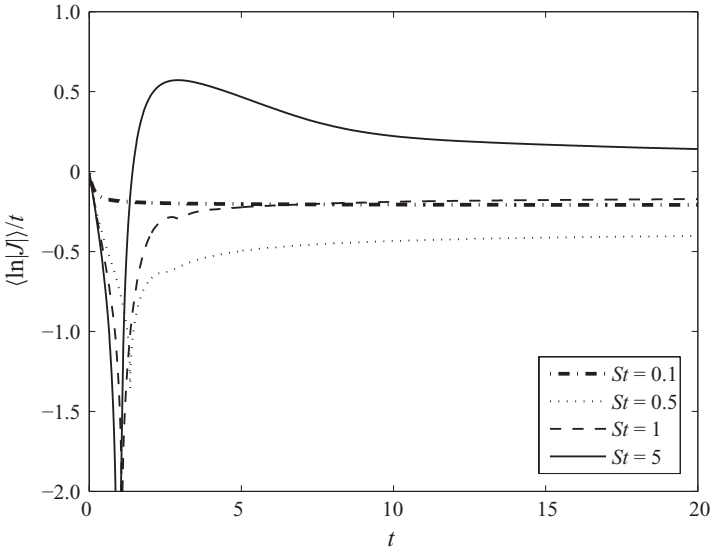

FIGURE 7. Rate-of-compression as a function of time for four different Stokes numbers, obtained in 10^5 different realizations of the non-isotropic random straining flow.

is that in this simple flow field (in which the particles are entirely transported by the underlying flow velocity) the segregation of particle would continue indefinitely: this, of course, ignores the absence of molecular or Brownian diffusion but nevertheless suggests that the concentration will be extremely high before Brownian diffusion can counteract the accumulation process. If $St = 5$, however, the compressibility approaches a positive value as $t \to \infty$, indicating that the particles are continuously occupying a larger volume in physical space. On the one hand, this is expressed in terms of an increased diffusion coefficient as seen in figure 4, on the other hand this corresponds to a significant decorrelation of particle velocities: two particles at almost the same position can have completely different velocities if St is large. A group of these particles that are released close together at $t = 0$, may quickly spread over different regions of the flow and thus the volume occupied by them, as measured by J, increases in the course of time.

The time-converged solution of $t^{-1}\langle \ln|J| \rangle$ is equal to the time-converged solution of $\langle \nabla \cdot \boldsymbol{v} \rangle$ (see (3.6)). We thus obtain $\langle \nabla \cdot \boldsymbol{v} \rangle$ by calculating J along a particle trajectory at a given Stokes number in 10^5 different realizations of the flow and determine the time-converged value of $t^{-1}\langle \ln|J| \rangle$, i.e. of $\langle \nabla \cdot \boldsymbol{v} \rangle$. The result is shown in figure 8 as a function of St, both for the isotropic random straining flow and for the non-isotropic random straining flow. If the Stokes number is smaller than a threshold value St_{cr}, $\langle \nabla \cdot \boldsymbol{v} \rangle$ is negative, which means that particles are continuously segregated: the segregation process continues indefinitely, and therefore the particles will be distributed on a pattern that becomes ever stringier in the course of time. For large Stokes numbers, $\langle \nabla \cdot \boldsymbol{v} \rangle$ approaches a positive value, in agreement with the curve for $St = 5$ in figure 7.

The results for the isotropic and the non-isotropic flow fields are very similar, indicating that in this work, the general picture of segregation is not altered qualitatively with the introduction of a distribution of length scales. However that being said, the influence of a broad range of scales as in real turbulence and the dependence of segregation on both Stokes and Reynolds numbers are not considered

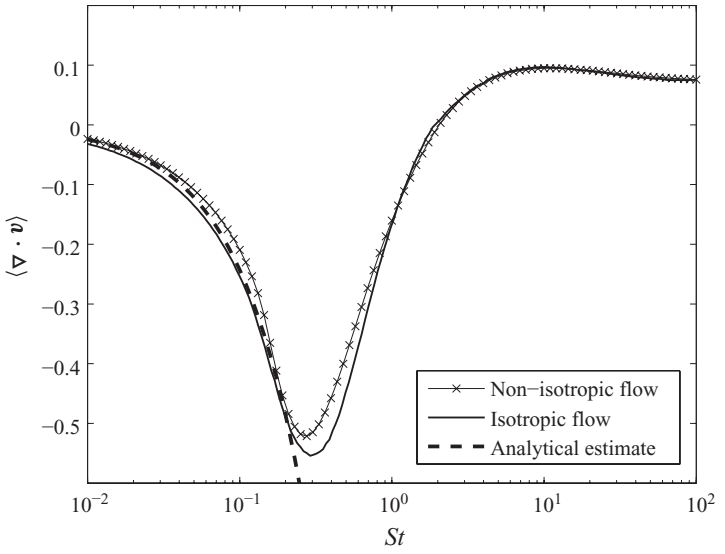

FIGURE 8. Time-converged solution for the compressibility $\langle \nabla \cdot \boldsymbol{v} \rangle$ as a function of the Stokes number, obtained from 10^5 different realizations of both the isotropic random straining flow and the non-isotropic random straining flow. For the sake of comparison, the analytical estimate valid for small Stokes numbers, i.e. $\langle \nabla \cdot \boldsymbol{v} \rangle = -24St/\pi^2$, is plotted as well.

here. In the isotropic flow, however, the negative peak of $\langle \nabla \cdot \boldsymbol{v} \rangle$ becomes more negative and is slightly shifted to the right with respect to the non-isotropic case. This bears some importance for real turbulent flows in which many different scales are present: it is expected that the segregation of particles is somewhat enhanced in a flow with a distribution of scales compared with a flow in which the only scale is present.

For small St, the compressibility of the particle phase is approximately linear in St. This is in accordance with the estimate given in (2.29), which is drawn in figure 8 for comparison. In both flow fields considered, the analytical estimate gives excellent results for $St < 0.25$. When the Stokes number becomes larger than 0.25, i.e. the Stokes number for which the value of J may pass through zero, then the analytical estimate is not valid anymore.

In figure 9, we show the variance of the compressibility as a function of the Stokes number. The variance is almost zero for small Stokes numbers, increases rapidly with St when $St > 0.25/S_0$, reaches a maximum for $St \simeq 0.7$ and decreases for larger values of St. The sudden increase in the variance with the Stokes number can be attributed to the fact that $|J|$ can only be equal to zero instantaneously for particles with $St > 0.25/S_0$ (see (3.7)). This is confirmed by the striking resemblance between figure 9 and figure 6, which indicates that the variance of the compressibility is indeed related to the presence of singularities in the particle concentration.

Figure 10(a) shows the skewness ($\mu_3/\mu_2^{3/2}$, where μ_k denotes the kth central moment) of the PDF of the compressibility of the particle phase. The PDF is negatively skewed for small Stokes numbers, with a sharp peak around $St = 0.25/S_0$. Thus, for these Stokes numbers the negative values of $(\nabla \cdot \boldsymbol{v} - \langle \nabla \cdot \boldsymbol{v} \rangle)$ are more likely to occur than positive values. For large Stokes numbers, however, the skewness goes to zero. This means that sudden collapses of the compressibility are on average equally likely to occur as sudden growths of the compressibility. This is in agreement with the phenomenon of particles overshooting the stagnation lines of the carrier flow:

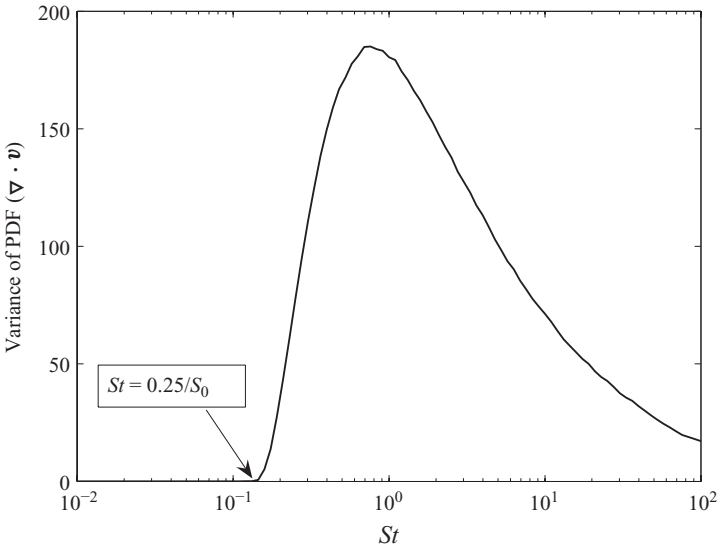

FIGURE 9. Time-converged solution for the variance of the PDF of $\nabla \cdot \boldsymbol{v}$ as a function of the Stokes number, obtained from 10^5 different realizations of the non-isotropic random straining flow.

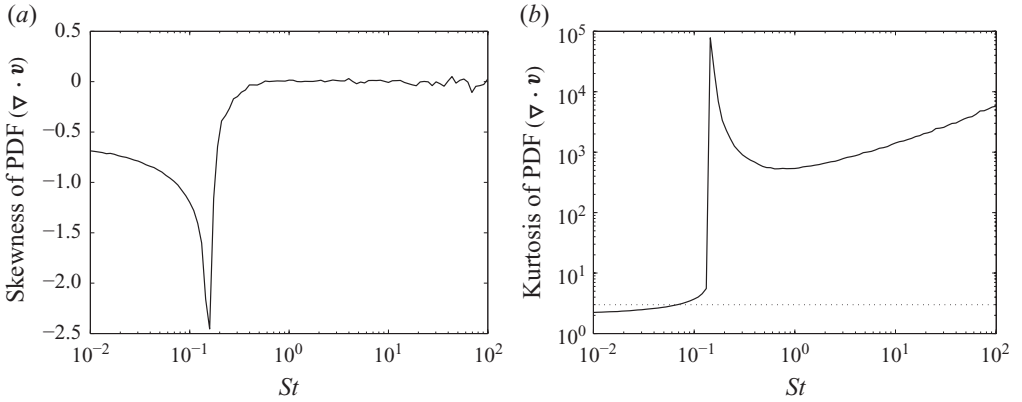

FIGURE 10. Time-converged solution for the skewness (a) and the kurtosis (b) of the PDF of $\nabla \cdot \boldsymbol{v}$ as a function of the Stokes number, obtained from 10^5 different realizations of the non-isotropic random straining flow. The kurtosis of a Gaussian distribution, 3, is shown as a dotted line for comparison.

instantaneously, the value of $|J|$ becomes equal to zero, and in the subsequent time step the value of $|J|$ has a finite value again.

The kurtosis (μ_4/μ_2^2) is shown in figure 10(b). It is approximately equal to 3 if $St < 0.25/S_0$, and suddenly increases as $St > 0.25/S_0$. Remarkably enough, the kurtosis is several orders of magnitude larger than 3 for the entire range of $St > 0.25/S_0$. Thus, the distribution is much wider than Gaussian and intermittent events are likely to occur. This emphasizes once more that extreme values of $\langle \nabla \cdot \boldsymbol{v} \rangle$ are related to events when J passes through zero.

3.3. *Lagrangian model for compressibility*

We mention briefly the results for particle behaviour in a simple Lagrangian model of a particle in a straining flow, for which the compressibility of the particle phase can be calculated analytically. We suppose that in a time step of constant value, 2τ say, a particle experiences a flow with a certain strain rate S in the x direction for a fixed time followed by a strain rate $-S$ for the same length of time. Thus, τ can be seen as the residence time of a particle inside a straining region. The strain rate experienced by the particle in the y direction is of course the opposite of the corresponding value in the x direction. This Lagrangian flow is similar to the Eulerian flow presented in § 2.1.1 except that in this Lagrangian case, the time for the change of sign of the strain rate is prescribed and therefore not dependent on the particle motion itself. The particle motion is now entirely linear and can be solved analytically within any given time step, given the initial conditions at the beginning of the time step. The purpose here is to show that the behaviour of this simple Lagrangian model has some of the features of the Eulerian model and, whilst this simple model is very efficient from a computational point of view, it also gives some insights into the statistics of the dispersion process. We note that the proposed Langrangian model is similar to a traditional random walk model in which the fluid velocity is constant during each time step (though random from one time step to the next).

The equations for the components J_{11} and J_{22} within a certain time interval $t_n \leqslant t < t_{n+1}$ ($t_n = 2\tau n$, $n \in \mathbb{N}$) can be written as follows:

$$\left.\begin{array}{ll} \ddot{J}_{11} + (\dot{J}_{11} - SJ_{11})/St = 0, & \ddot{J}_{22} + (\dot{J}_{22} + SJ_{22})/St = 0, \quad t_n \leqslant t < t_n + \tau; \\ \ddot{J}_{11} + (\dot{J}_{11} + SJ_{11})/St = 0, & \ddot{J}_{22} + (\dot{J}_{22} - SJ_{22})/St = 0, \quad t_n + \tau \leqslant t < t_n + 2\tau. \end{array}\right\} \tag{3.8}$$

Since the above equations are linear ordinary differential equations, solutions for J_{11}, $\dot{J}_{11}$, J_{22} and $\dot{J}_{22}$ at time t_{n+1} can be calculated analytically, as a function of the values of J_{11}, $\dot{J}_{11}$, J_{22} and $\dot{J}_{22}$ at time t_n:

$$\begin{bmatrix} J_{11}(t_{n+1}) \\ \dot{J}_{11}(t_{n+1}) \end{bmatrix} = [\boldsymbol{A}^-][\boldsymbol{A}^+] \begin{bmatrix} J_{11}(t_n) \\ \dot{J}_{11}(t_n) \end{bmatrix}, \qquad \begin{bmatrix} J_{22}(t_{n+1}) \\ \dot{J}_{22}(t_{n+1}) \end{bmatrix} = [\boldsymbol{A}^+][\boldsymbol{A}^-] \begin{bmatrix} J_{22}(t_n) \\ \dot{J}_{22}(t_n) \end{bmatrix}, \tag{3.9}$$

where

$$[\boldsymbol{A}^\pm] \equiv \begin{bmatrix} \dfrac{\lambda_2^\pm}{\lambda_2^\pm - \lambda_1^\pm}\exp(\lambda_1^\pm\tau) + \dfrac{\lambda_1^\pm}{\lambda_1^\pm - \lambda_2^\pm}\exp(\lambda_2^\pm\tau) & \dfrac{1}{\lambda_1^\pm - \lambda_2^\pm}\exp(\lambda_1^\pm\tau) + \dfrac{1}{\lambda_2^\pm - \lambda_1^\pm}\exp(\lambda_2^\pm\tau) \\ \dfrac{\lambda_1^\pm\lambda_2^\pm}{\lambda_2^\pm - \lambda_1^\pm}\exp(\lambda_1^\pm\tau) + \dfrac{\lambda_1^\pm\lambda_2^\pm}{\lambda_1^\pm - \lambda_2^\pm}\exp(\lambda_2^\pm\tau) & \dfrac{\lambda_1^\pm}{\lambda_1^\pm - \lambda_2^\pm}\exp(\lambda_1^\pm\tau) + \dfrac{\lambda_2^\pm}{\lambda_2^\pm - \lambda_1^\pm}\exp(\lambda_2^\pm\tau) \end{bmatrix}, \tag{3.10}$$

and $\lambda_i^\pm$ given in (3.4). It is noted that (3.9) is valid for all Stokes numbers, i.e. also when $St > 0.25/S$ making λ_1^- and λ_2^- complex.

We note that (3.9) is a recurrence relation which can be reformulated as follows:

$$\frac{\dot{J}_{11}(t_{n+1})}{J_{11}(t_{n+1})} = \frac{\zeta_{21}^+ + \zeta_{22}^+\big(\dot{J}_{11}(t_n)/J_{11}(t_n)\big)}{\zeta_{11}^+ + \zeta_{12}^+\big(\dot{J}_{11}(t_n)/J_{11}(t_n)\big)}, \qquad \frac{\dot{J}_{22}(t_{n+1})}{J_{22}(t_{n+1})} = \frac{\zeta_{21}^+ + \zeta_{22}^+\big(\dot{J}_{22}(t_n)/J_{22}(t_n)\big)}{\zeta_{11}^+ + \zeta_{12}^+\big(\dot{J}_{22}(t_n)/J_{22}(t_n)\big)}, \tag{3.11}$$

where $[\boldsymbol{\zeta}^+] \equiv [\boldsymbol{A}^-][\boldsymbol{A}^+]$ and $[\boldsymbol{\zeta}^-] \equiv [\boldsymbol{A}^+][\boldsymbol{A}^-]$. After a sufficiently long time, (3.11) approaches a steady solution. These steady values of $(\dot{J}_{11}/J_{11})$ and $(\dot{J}_{22}/J_{22})$ can be

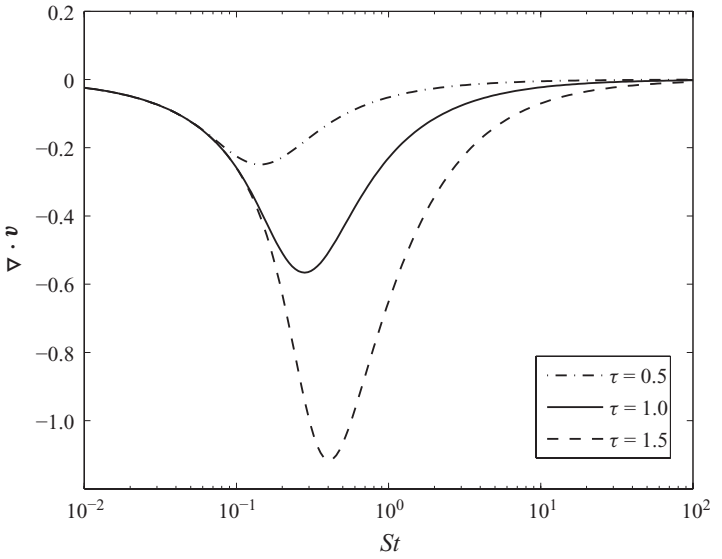

FIGURE 11. Long-term compressibility $\nabla \cdot \boldsymbol{v}$ as a function of the Stokes number in a simple random walk model, obtained by solving (3.12) analytically for three different values of the residence time τ. The strain rate $S = \sqrt{12}/\pi$.

obtained from the quadratic polynomials:

$$\beta_{12}^{+}\left(\frac{\dot{J}_{11}}{J_{11}}\right)^2 + (\zeta_{11}^{+} - \zeta_{22}^{+})\left(\frac{\dot{J}_{11}}{J_{11}}\right) - \zeta_{21}^{+} = 0, \quad \zeta_{12}^{-}\left(\frac{\dot{J}_{22}}{J_{22}}\right)^2 + (\zeta_{11}^{-} - \zeta_{22}^{-})\left(\frac{\dot{J}_{22}}{J_{22}}\right) - \zeta_{21}^{-} = 0. \tag{3.12}$$

From this equation, we calculate the long-term value of $(\dot{J}_{11}/J_{11})$ and $(\dot{J}_{22}/J_{22})$; since (3.12) is a quadratic polynomial, it gives two results for both $(\dot{J}_{11}/J_{11})$ and $(\dot{J}_{22}/J_{22})$ of which only the highest values have a physical meaning and are taken into account. Then, we determine the long-term rate-of-compression as follows: $\mathrm{d}(\ln|J|)/\mathrm{d}t = \mathrm{d}(\ln|J_{11}|)/\mathrm{d}t + \mathrm{d}(\ln|J_{22}|)/\mathrm{d}t = (\dot{J}_{11}/J_{11}) + (\dot{J}_{22}/J_{22})$, which is equal to $\nabla \cdot \boldsymbol{v}$ (see (2.26)). The result is shown in figure 11 as a function of the Stokes number, for three different values of the residence time τ. The strain rate is kept constant at $S = \sqrt{12}/\pi$, allowing comparison with the non-isotropic random flow field presented in § 2.1.1 in which the root-mean-square strain rate is $\sqrt{12}/\pi$ as well.

Figure 11 shows long-term values of the compressibility of the particle phase, $\nabla \cdot \boldsymbol{v}$, determined analytically from (3.12). A constant negative value of the compressibility is consistent with an accumulation of particles at the end of each time step. The minimum value is situated around $0.1 < St < 1$ as in the case of the mean compressibility in the Eulerian flow field, presented in figure 8. In general, the dependence of the compressibility on the Stokes number is very well captured by the present simple model.

The results presented in figure 11 indicate that the Stokes number for which the highest compressibility is observed, increases with higher values of the Lagrangian time scale τ. This can be explained as follows: if τ is larger, the particles are given more time to adapt to the flow. Thus, they have more time to accumulate before they have to adapt to a new flow field in which the strain rate is opposite. In brief,

for higher values of τ, the 'time of accumulation' increases relatively to the 'time of adaptation'. For very small Stokes numbers ($St < 0.05$), the value of $\nabla \cdot \boldsymbol{v}$ is not visibly altered for the three values of τ chosen, since small particles adapt to the flow relatively quickly. Therefore their 'time of adaptation' is short with respect to the 'time of accumulation' for all $\tau \gg 0.05$.

3.4. *Random uncorrelated motion*

We determine the RUM of inertial particles by measuring the contribution it makes to the particle kinetic energy per unit mass. For this purpose, we calculate the particle pair velocity correlation R_{xx} as a function of particle separation in the non-isotropic random straining flow, defined as

$$R_{xx}(\Delta x) = \frac{\langle v_x^{(1)} v_x^{(2)} \big| \boldsymbol{x}^{(1)} - \boldsymbol{x}^{(2)} = \boldsymbol{e}_x \Delta x \rangle_{12}}{\langle v_x^2 \rangle}, \tag{3.13}$$

where (1) and (2) refer to two particles at a certain moment in time in one particular realization of the flow. The brackets '$\langle\ \rangle_{12}$' denote an average over all particle pairs in all realizations, as opposed to the brackets '$\langle\ \rangle$' which denote an average over all particles in all realizations. For accuracy versus computation time, we chose 10^3 particles and 10^2 realizations of the flow.

At the start of each simulation, all 10^3 particles are uniformly distributed inside the lattice cell of size $2\pi \times 2\pi$, with a velocity equal to the local fluid velocity. Periodic boundary conditions are imposed for the particle motion at the edges of the lattice cell; this requires no approximation since the non-isotropic random straining flow is always periodic in space with length 2π. Periodicity of the particle motion and homogeneity means that the following expressions are valid:

$$R_{xx}(\Delta x) = R_{xx}(-\Delta x) = R_{xx}(2\pi - \Delta x) = R_{yy}(\Delta y). \tag{3.14}$$

Thus, in order to obtain all relevant information on R_{xx} and R_{yy}, it is sufficient to calculate $R_{xx}(\Delta x)$ for $0 \leqslant \Delta x < \pi$ only.

The correlation for fluid particles $R_{xx,fp}(\Delta x)$ can be calculated analytically from the equations of motion of the flow field, (2.4):

$$R_{xx,fp}(\Delta x) = \frac{1}{\overline{u_x^2}^*} \int_{lattice} \overline{u_x(x, y) u_x(x + \Delta x, y)}^* \, \mathrm{d}x \, \mathrm{d}y. \tag{3.15}$$

Due to (3.14), it is sufficient to consider only one lattice cell of size $\pi \times \pi$, whose left lower corner is taken to coincide with the origin for convenience. Then, (3.15) becomes

$$R_{xx,fp}(\Delta x) = \frac{1}{\pi^2 \overline{u_x^2}^*} \int_0^\pi \int_0^\pi \overline{u_x(x, y) u_x(x + \Delta x, y)}^* \, \mathrm{d}x \, \mathrm{d}y. \tag{3.16}$$

Because $\overline{u_x^2}^* = 1$ and $\overline{S^2}^* = 12/\pi^2$, and because the integrand is independent of y, we arrive at the following expression for $R_{xx,fp}(\Delta x)$:

$$R_{xx,fp}(\Delta x) = \frac{12}{\pi^3} \int_0^{\pi - \Delta x} \left(x - \frac{\pi}{2}\right)\left(x + \Delta x - \frac{\pi}{2}\right) \mathrm{d}x + \int_{\pi - \Delta x}^{\pi} \left(x - \frac{\pi}{2}\right)\left(\frac{3\pi}{2} - x - \Delta x\right) \mathrm{d}x, \tag{3.17}$$

which has as solution:

$$R_{xx,fp}(\Delta x) = 1 - \frac{6}{\pi^2} \Delta x^2 + \frac{4}{\pi^3} \Delta x^3 \quad \text{for} \quad 0 \leqslant \Delta x \leqslant \pi. \tag{3.18}$$

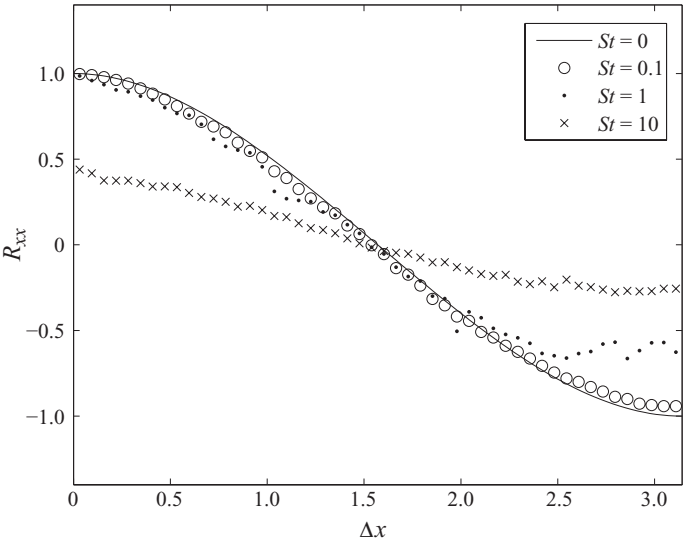

FIGURE 12. The two-point one-time velocity correlation of inertial particles with three different Stokes numbers in the non-isotropic random strain flow, plotted as a function of the particle separation Δx. The velocity correlations between 10^3 particles are measured at time $t = 100$ in 10^2 separate realizations of the flow field. The solid line indicates the analytical solution for the velocity correlation of fluid particles, $R_{xx,fp}$, given in (3.18).

We calculate the correlation coefficient $R_{xx}(\Delta x)$ for inertial particles by evaluating the positions and velocities of 10^3 particles within the domain $[0 \leqslant \Delta x < 2\pi, 0 \leqslant y < 2\pi]$ at a time $t = 100$. The domain is divided up into 100 bins of 0.02π dimension in the y direction, the i_yth bin being the bin whose centre is at $y = 0.02\pi(i_y - \frac{1}{2})$ where $i_y = 1, \ldots, 100$. For each particle pair whose y coordinates satisfy $0.02\pi(i_y - 1) \leqslant y^{(1)} < 0.02\pi i_y$ and $0.02\pi(i_y - 1) \leqslant y^{(2)} < 0.02\pi i_y$, we evaluate the separation Δx and calculate $v_x^{(1)} v_x^{(2)}$. After sorting all particle pairs into suitable bins, we then repeat this procedure for 10^2 realizations of the carrier flow and average over all particle pairs within each bin to give the value $\langle v_x^{(1)} v_x^{(2)} \big| \boldsymbol{x}^{(1)} - \boldsymbol{x}^{(2)} = \boldsymbol{e}_x \Delta x \rangle_{12}$. In addition we calculate $\langle v_x^2 \rangle$ by summing v_x^2 over all 10^3 particles in the domain and over 10^2 realizations of the flow field and then dividing by $10^3 \times 10^2$, finally to obtain $R_{xx}(\Delta x)$ using (3.13).

Because the particle concentration is initially uniform, the particle pair correlation is identical to the Eulerian spatial velocity correlation of fluid particles, given by (3.18). In the course of time, the velocity correlation of inertial particles deviates from the fluid particle correlation due to inertia effects. After a sufficiently long time, $R_{xx}(\Delta x)$ reaches a time-converged solution within some statistical error. This time-converged solution is shown in figure 12, for three different values of the Stokes number. The correlation for fluid particles, given in (3.18) is shown as well (solid line with $St = 0$). It is apparent that the case for $St = 0.1$ is almost identical to the pair separation correlation of fluid particles. For the other cases, the curves are noticeably different, with the most interesting property of all, that the extrapolated values for $\Delta x = 0$ are not equal to unity, unlike the graphs for $St = 0$ and $St = 0.1$. This is most marked for $St = 10$. The difference between the extrapolated value and unity represents the contribution of RUM to the particle kinetic energy:

$$\text{RUM} \equiv 1 - \lim_{\Delta x \to 0} R_{xx}(\Delta x). \tag{3.19}$$

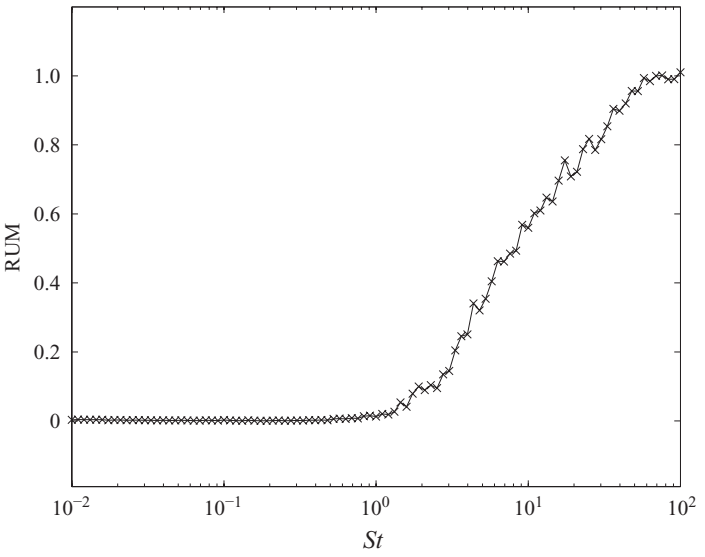

FIGURE 13. The random uncorrelated component of the particle kinetic energy (RUM) as a function of the Stokes number in the non-isotropic random straining flow. For each Stokes number, the result is obtained by measuring the two-point velocity correlations of 10^3 particles after time $t = 100$ in 10^2 separate realizations of the flow field.

Figure 13 shows the values of RUM at $t = 100$ as a function of St. We note that there is no real measurable contribution from RUM if $St < 1$. Thus, these particles are very well correlated. If $St > 1$, however, the velocity decorrelation becomes noticeable. For these Stokes numbers, all realizable states correspond to a sequence of lightly damped oscillators with $St > 0.25/S$ for almost all possible values of S. This result provides an explanation for why the compressibility, $\langle \boldsymbol{\nabla} \cdot \boldsymbol{v} \rangle$ shown in figure 8, suddenly increases as $St > 1$.

4. Dispersion and segregation of particles in a flow field composed of random Fourier modes

In this section, we present and discuss the results obtained for the flow field composed of 200 random Fourier modes introduced in § 2.2. Just as in the case of the random straining flow discussed in § 3, we focus our attention on the segregation of particles and on the occurrence of RUM.

The trajectory of each particle is calculated from (2.16) by using a fourth-order Runge–Kutta method with a time step of 0.01. The carrier flow velocity at the position of the particle is computed from (2.12). Since the carrier flow field is defined for all $\boldsymbol{x}$, the fluid velocity at the position of a particle and its gradients can be calculated exactly, without interpolation. In all simulations, the initial velocity of a particle is taken equal to the local velocity of the carrier flow.

4.1. *Compressibility of the particle phase*

In order to determine the compressibility of the particle phase as a continuum, we calculate the trajectories of 10 000 particles which are uniformly distributed over the domain at $t = 0$. Along each particle trajectory, (2.20) is solved simultaneously for all components J_{ij} using a fourth-order Runge–Kutta method. Subsequently, the value of $J = \det(J_{ij})$ is calculated after each time step.

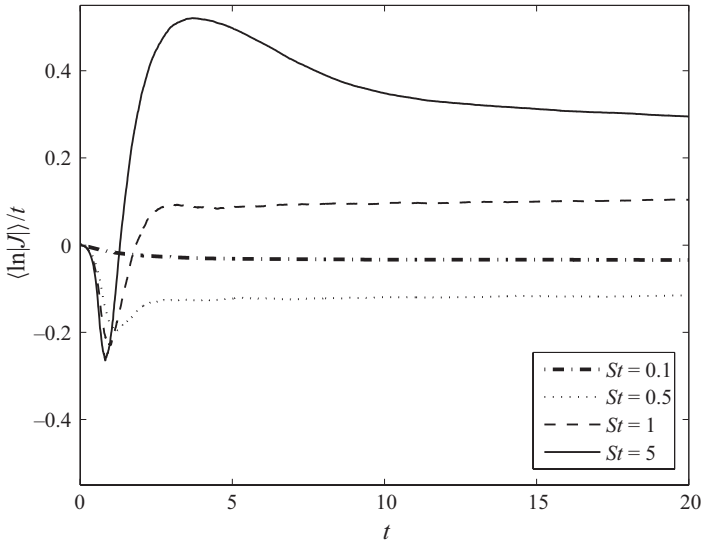

FIGURE 14. The particle-averaged rate-of-compression, $t^{-1}\langle \ln|J|\rangle$, as a function of time in the flow field composed of random Fourier modes, for four different values of the Stokes number.

In figure 14, the results for the particle-averaged rate-of-compression $t^{-1}\langle \ln|J|\rangle$ are shown as a function of time, for four different Stokes numbers. The Stokes numbers chosen are the same as in figure 7, so that the results from the present flow field can be compared to the results previously obtained for the non-isotropic random straining flow. For small Stokes numbers, such as $St = 0.1$, $t^{-1}\langle \ln|J|\rangle$ approaches a constant negative value. When the Stokes number increases, the value of $t^{-1}\langle \ln|J|\rangle$ becomes more negative, as is illustrated by the line for $St = 0.5$. Thus, the process of segregation is enhanced with larger Stokes numbers provided the Stokes number is sufficiently small. For relatively large Stokes numbers such as $St = 1$ or $St = 5$, however, $t^{-1}\langle \ln|J|\rangle$ approaches a positive value when $t \to \infty$. This means that a group of particles, released at $t = 0$ at infinitesimally small distances from each other, occupies an increasingly large volume in the course of time. It is an indication of the fact that the velocities of nearby particles becomes less correlated as St increases, as we will show in § 4.3. It is noted that figure 14 has not altered qualitatively with respect to figure 7; apparently, the observed behaviour for $\ln|J|$ in the course of time is similar in different models of turbulent flows, and not due to special characteristics of a specific model.

Figure 15(a) shows the results of $\lim_{t\to\infty} t^{-1}\langle \ln|J|\rangle$ for a wide range of values of Stokes numbers. It is noted that this value is equal to $\lim_{t\to\infty}\langle \nabla\cdot\boldsymbol{v}\rangle$, i.e. the time-converged compressibility of the particle velocity field. Just like in the case of figure 8, a critical value of the Stokes number can be determined, St_{cr}; in the present case, $St_{cr} \simeq 0.7$. If the particle Stokes number is lower than St_{cr}, then the particle velocity field is continuously compressed in the course of time and the process of segregation continues indefinitely. If, on the other hand, the Stokes number is larger than St_{cr}, $\langle \nabla\cdot\boldsymbol{v}\rangle$ continuously increases and the particles are mixed.

The dependence of the time-converged value of $\langle \nabla\cdot\boldsymbol{v}\rangle$ upon the Stokes number is illustrated in figure 15(b), for $St < St_{cr}$. Apparently, $\langle \nabla\cdot\boldsymbol{v}\rangle$ is approximately proportional to St^2. This can be explained as follows. The time-converged

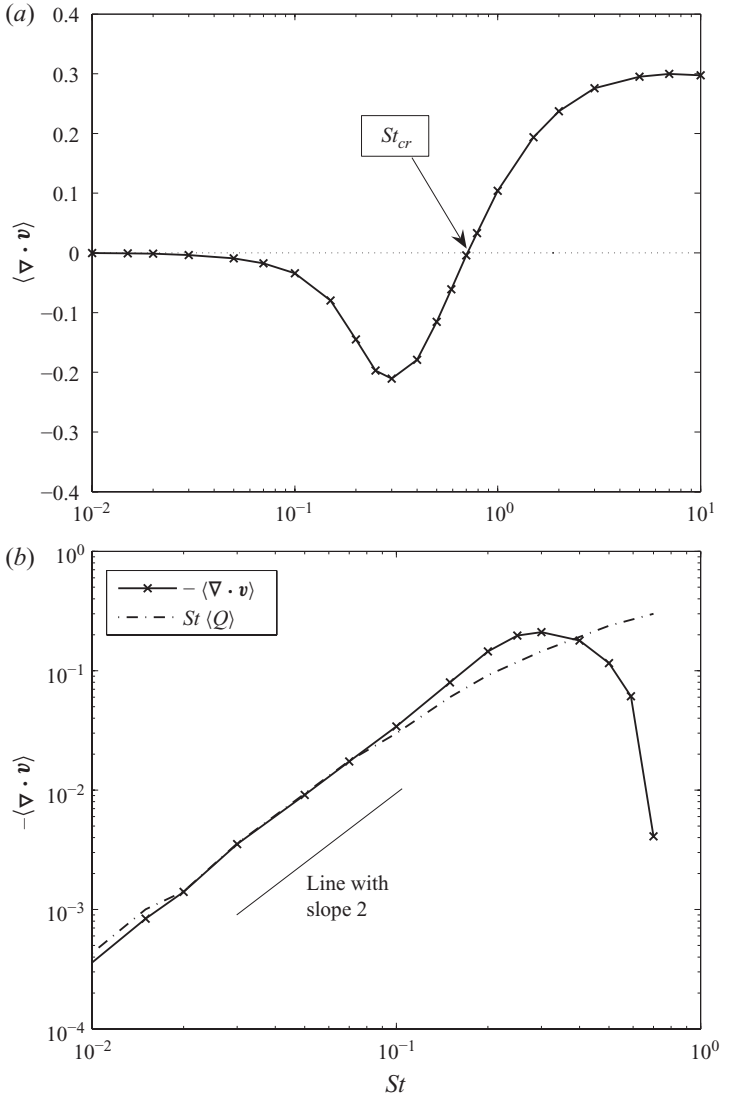

FIGURE 15. Converged results for the particle-averaged compressibility of the particle velocity field in the flow field composed of random Fourier modes as a function of St, plotted on a semi-log scale (a), and on a log-log scale (b). Figure (b) also shows $St\langle Q \rangle$ (the leading-order term in the analytical estimate given in (4.1)), and a line proportional to St^2.

compressibility, averaged over all particles, can be estimated using (2.27):

$$\langle \nabla \cdot \boldsymbol{v} \rangle \simeq -St\langle Q \rangle + St^2 \frac{\mathrm{d}\langle Q \rangle}{\mathrm{d}t} + O(St^3). \tag{4.1}$$

Since the value of $\langle \nabla \cdot \boldsymbol{v} \rangle$ goes to a constant as $t \to \infty$, it must hold that $\langle Q \rangle \to$ constant and $\mathrm{d}\langle Q \rangle / \mathrm{d}t = 0$ as well; this is confirmed by our numerical simulations where we measure Q along each particle trajectory and subsequently average this value over all particles. In a certain given flow field that is statistically stationary and homogeneous, the long-time value of $\langle Q \rangle$ can only be a function of the Stokes number St. A Taylor

expansion of $\langle Q\rangle$ around $St=0$ (passive tracer limit) gives

$$\langle Q\rangle(St)=\langle Q\rangle(0)+St\left.\frac{\mathrm{d}\langle Q\rangle}{\mathrm{d}St}\right|_{St=0}+O(St^2)=\langle Q\rangle_{fp}+St\left.\frac{\mathrm{d}\langle Q\rangle}{\mathrm{d}St}\right|_{St=0}+O(St^2), \quad (4.2)$$

where '$\langle\ \rangle_{fp}$' denotes an average over fluid particles. $\langle Q\rangle_{fp}$ can be calculated by taking the integral over the whole domain of $Q(\boldsymbol{x},t)$, which can be derived directly from (2.12) and (2.28):

$$\begin{aligned}\langle Q\rangle_{fp}=\frac{1}{\mathscr{L}^3}\int_0^{\mathscr{L}}\int_0^{\mathscr{L}}\int_0^{\mathscr{L}}\sum_{m=1}^{N}\sum_{n=1}^{N}\Big[&c_{11}^{(m,n)}\cos(\boldsymbol{k}^+\cdot\boldsymbol{x}+\omega^+t)+c_{12}^{(m,n)}\sin(\boldsymbol{k}^+\cdot\boldsymbol{x}+\omega^+t)\\&+c_{21}^{(m,n)}\cos(\boldsymbol{k}^-\cdot\boldsymbol{x}+\omega^-t)+c_{22}^{(m,n)}\sin(\boldsymbol{k}^-\cdot\boldsymbol{x}+\omega^-t)\Big]\mathrm{d}\boldsymbol{x}, \quad (4.3)\end{aligned}$$

where $\boldsymbol{k}^+\equiv\boldsymbol{k}^{(m)}+\boldsymbol{k}^{(n)}$, $\boldsymbol{k}^-\equiv\boldsymbol{k}^{(m)}-\boldsymbol{k}^{(n)}$, $\omega^+\equiv\omega^{(m)}+\omega^{(n)}$ and $\omega^-\equiv\omega^{(m)}-\omega^{(n)}$, and the coefficients $c_{ij}^{(m,n)}$ are

$$\begin{aligned}c_{11}^{(m,n)}\equiv\frac{1}{2|\boldsymbol{k}^{(m)}||\boldsymbol{k}^{(n)}|}\Big[&-\big(\big(\boldsymbol{a}^{(m)}\times\boldsymbol{k}^{(m)}\big)\cdot\boldsymbol{k}^{(n)}\big)\big(\big(\boldsymbol{a}^{(n)}\times\boldsymbol{k}^{(n)}\big)\cdot\boldsymbol{k}^{(m)}\big)\\&+\big(\big(\boldsymbol{b}^{(m)}\times\boldsymbol{k}^{(m)}\big)\cdot\boldsymbol{k}^{(n)}\big)\big(\big(\boldsymbol{b}^{(n)}\times\boldsymbol{k}^{(n)}\big)\cdot\boldsymbol{k}^{(m)}\big)\Big],\\c_{12}^{(m,n)}\equiv\frac{-1}{2|\boldsymbol{k}^{(m)}||\boldsymbol{k}^{(n)}|}\Big[&\big(\big(\boldsymbol{b}^{(m)}\times\boldsymbol{k}^{(m)}\big)\cdot\boldsymbol{k}^{(n)}\big)\big(\big(\boldsymbol{a}^{(n)}\times\boldsymbol{k}^{(n)}\big)\cdot\boldsymbol{k}^{(m)}\big)\\&+\big(\big(\boldsymbol{a}^{(m)}\times\boldsymbol{k}^{(m)}\big)\cdot\boldsymbol{k}^{(n)}\big)\big(\big(\boldsymbol{b}^{(n)}\times\boldsymbol{k}^{(n)}\big)\cdot\boldsymbol{k}^{(m)}\big)\Big],\\c_{21}^{(m,n)}\equiv\frac{1}{2|\boldsymbol{k}^{(m)}||\boldsymbol{k}^{(n)}|}\Big[&\big(\big(\boldsymbol{a}^{(m)}\times\boldsymbol{k}^{(m)}\big)\cdot\boldsymbol{k}^{(n)}\big)\big(\big(\boldsymbol{a}^{(n)}\times\boldsymbol{k}^{(n)}\big)\cdot\boldsymbol{k}^{(m)}\big)\\&+\big(\big(\boldsymbol{b}^{(m)}\times\boldsymbol{k}^{(m)}\big)\cdot\boldsymbol{k}^{(n)}\big)\big(\big(\boldsymbol{b}^{(n)}\times\boldsymbol{k}^{(n)}\big)\cdot\boldsymbol{k}^{(n)}\big)\Big],\\c_{22}^{(m,n)}\equiv\frac{1}{2|\boldsymbol{k}^{(m)}||\boldsymbol{k}^{(n)}|}\Big[&-\big(\big(\boldsymbol{a}^{(m)}\times\boldsymbol{k}^{(m)}\big)\cdot\boldsymbol{k}^{(n)}\big)\big(\big(\boldsymbol{b}^{(n)}\times\boldsymbol{k}^{(n)}\big)\cdot\boldsymbol{k}^{(m)}\big)\\&+\big(\big(\boldsymbol{b}^{(m)}\times\boldsymbol{k}^{(m)}\big)\cdot\boldsymbol{k}^{(n)}\big)\big(\big(\boldsymbol{a}^{(n)}\times\boldsymbol{k}^{(n)}\big)\cdot\boldsymbol{k}^{(m)}\big)\Big].\end{aligned}$$

It is clear that the coefficients $c_{ij}^{(m,n)}$ are all 0 if $m=n$. All other terms in (4.3) vanish if we integrate over the entire domain due to the fact that $\int_0^{\mathscr{L}}\sin(\kappa x)\,\mathrm{d}x=0$ and $\int_0^{\mathscr{L}}\cos(\kappa x)\mathrm{d}x=0$, if $\kappa\mathscr{L}/2\pi\in\mathbb{N}$. Therefore, we have

$$\langle Q\rangle_{fp}=\frac{1}{\mathscr{L}^3}\int_0^{\mathscr{L}}\int_0^{\mathscr{L}}\int_0^{\mathscr{L}}Q(\boldsymbol{x},t)\,\mathrm{d}\boldsymbol{x}=0, \quad \forall \quad t. \quad (4.4)$$

It is worth noting that this result is due to the incompressibility, the differentiability and the periodicity of the flow field. Therefore, $\langle Q\rangle_{fp}=0$ in the case of homogeneous isotropic turbulence as well. It is not necessarily true, however, that $\langle Q\rangle_{fp}=0$ in any flow field in reality or in numerical simulations. To give just one example, in the random straining flow field presented in § 2.1 we have $\langle Q\rangle_{fp}=2S^2\neq 0$, and thus $\langle\nabla\cdot\boldsymbol{v}\rangle\propto St$ according to (4.1) and (4.2), which is confirmed by figure 8. Also many phenomena of clustering of inertial particles in non-homogeneous flows (e.g. Marcu *et al.* 1995; IJzermans, Hagmeijer & van Langen 2007) can be related ultimately to the fact that Q is non-zero in regions of the flow where inertial particles accumulate;

in these flows the compressibility of the particle velocity field is proportional to St, not to St^2.

Inserting the result from (4.4) into (4.2) gives

$$\langle Q\rangle(St) = St\left.\frac{\mathrm{d}\langle Q\rangle}{\mathrm{d}St}\right|_{St=0} + O(St^2). \tag{4.5}$$

Because inertial particles with a small but non-zero Stokes number are well known to preferentially concentrate in strain regions (Maxey 1987), it is clear that

$$\left.\frac{\mathrm{d}\langle Q\rangle}{\mathrm{d}St}\right|_{St=0} > 0. \tag{4.6}$$

Inserting this into (4.2) shows that $\langle Q\rangle \propto St$, so that the approximation given in (4.1) indicates that

$$\langle \nabla\cdot\boldsymbol{v}\rangle = -CSt^2 + O(St^3), \tag{4.7}$$

with C a positive constant. In figure 15(b), the proportionality of $\langle \nabla\cdot\boldsymbol{v}\rangle$ to St^2 is clearly visible. The observation that the compressibility is proportional to St^2, or alternatively that $\langle Q\rangle \propto St$, is in agreement with the results obtained previously by, for example, Bec (2005) in numerical simulations of periodic smoothly varying flow fields and by Chun *et al.* (2005) in DNS of homogeneous isotropic turbulence.

4.2. *Statistics of the particle number density*

Now we investigate the statistics of the particle number density in the course of time. The moments of the particle number density can be determined from (2.24). The result for four values of α is presented in figure 16, for (a) $St = 0.05$ and (b) $St = 0.5$. In both cases the value of $\overline{n^0}$, which corresponds to $\langle |J|\rangle$, remains equal to unity for all time, as expected. In addition, it follows directly from (2.24) that $\overline{n^1} = \langle |J|^0\rangle = 1$. The other moments of the particle number density are markedly higher than 1 and are associated with the non-uniformity in the spatial distribution of particles.

There is a qualitative distinction between the cases of small Stokes numbers such as $St = 0.05$ in figure 16(a), and large Stokes numbers such as $St = 0.5$ in figure 16(b). If the Stokes number is large, it may happen that $|J| = 0$ for a particle due to the crossing of trajectories. These intermittent events, which cause $n \to \infty$, dominate the statistics of higher-order moments of the PDF at certain moments in time, as is reflected by the spikes in the curve for $St = 0.5$ in figure 16(b). Hence, the spatial distribution of particles in a random turbulence-like flow may be highly intermittent.

However, for sufficiently small Stokes numbers where RUM is not important (such as $St = 0.05$ in figure 16a), we observe that $\overline{n^\alpha}$ depends exponentially on time and

$$\overline{n^\alpha} \propto \exp(\gamma t), \tag{4.8}$$

where γ is a function of α and St. As can be seen in figure 16(a), the higher-order moments grow faster than the lower-order moments. This demonstrates unambiguously that the segregation process continues indefinitely in this case where $St = 0.05$.

By repeating the calculation of $\overline{n^\alpha}$ over a range of Stokes numbers, we can determine the factor γ as a function of St and α; the result is shown in figure 17(a). The curved shape of the surface depicting γ is in agreement with Balkovsky *et al.* (2001) who

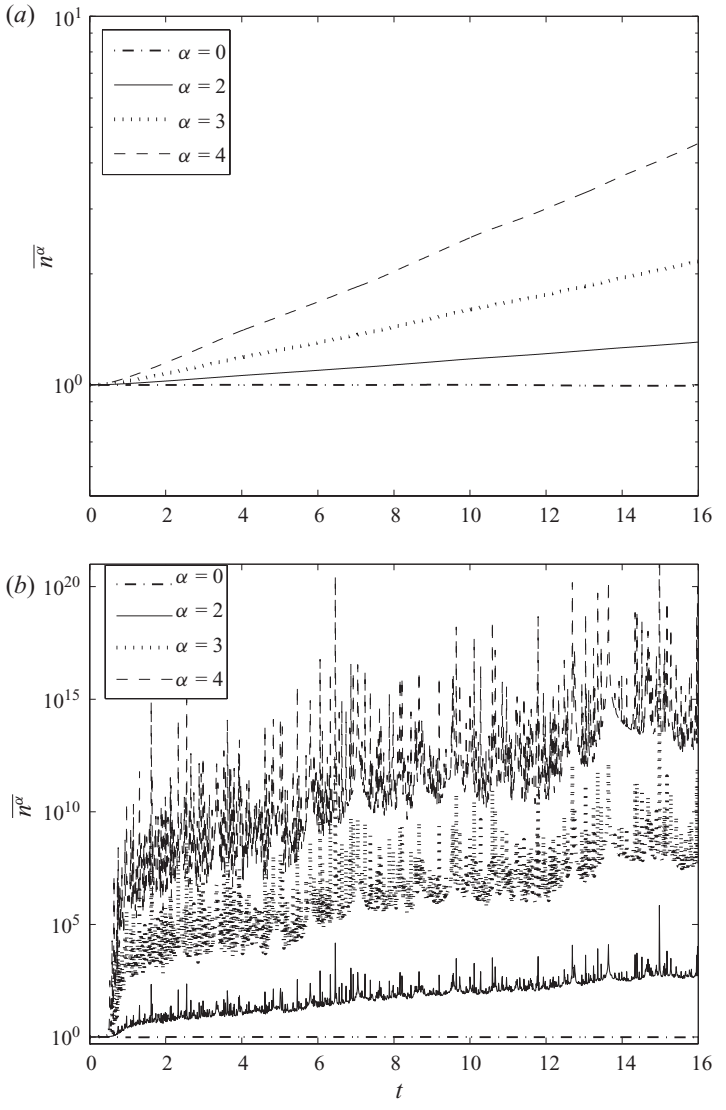

FIGURE 16. Spatial average of the αth moment of the particle number density $\overline{n^\alpha}$ for four values of α; (*a*) $St = 0.05$; (*b*) $St = 0.5$.

predicted theoretically that in turbulent flows γ is a convex function of α at constant St, i.e. $\partial^2\gamma/\partial\alpha^2 \neq 0 \ \forall \ \alpha$. Indeed, we see that $\gamma < 0$ if $0 < \alpha < 1$, and $\gamma > 0$ if $\alpha < 0$ or $\alpha > 1$.

In figure 17(*b*), we show the factor γ as a function of the Stokes number, for five different values of α. The lines in figure 17(*b*) are in fact cuts through the surface depicted in figure 17(*a*) at constant α. Apparently, the spatially averaged moments of the particle number density are proportional to St^2. This is in agreement with our theoretical analysis presented in § 4.1 and the estimate for the compressibility of the particle phase given in (4.7).

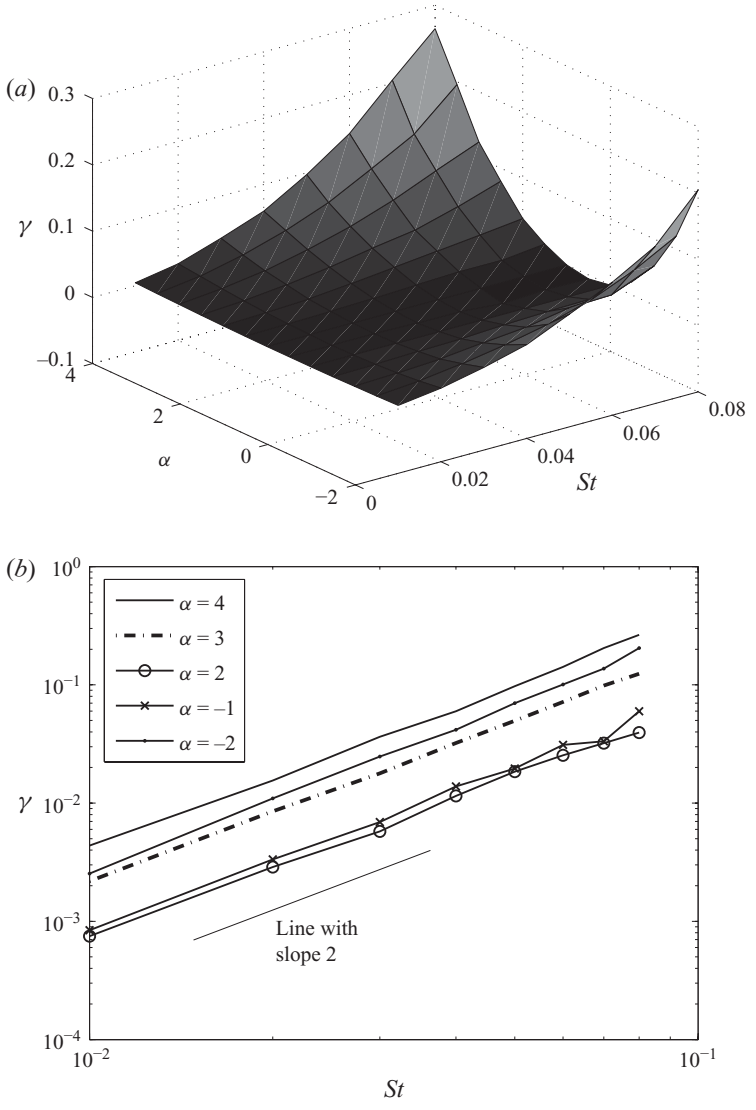

FIGURE 17. (*a*) Factor γ, which appears (4.8), as a function of St and α. (*b*) Factor γ as a function of St, for five different values of α.

4.3. *Random uncorrelated motion*

In this section, we investigate the velocity correlations between particles in the flow composed of 200 random Fourier modes. Particular attention is paid to RUM, i.e. the random uncorrelated component of the kinetic energy of the particles. For this purpose, the correlation between the velocities of two inertial particles is calculated.

In order to obtain accurate results for the velocity correlation between particles, we make use of the periodicity of the flow as follows. Let the separation vector between two particles (labelled '1' and '2') be denoted by: $\boldsymbol{r}_{12} = \boldsymbol{x}^{(1)} - \boldsymbol{x}^{(2)}$. If the distance between two particles in the x direction is larger than half the size of the physical domain, i.e. $|\boldsymbol{r}_{12} \cdot \boldsymbol{e}_x| > \mathscr{L}/2$, then $\boldsymbol{r}_{12} \cdot \boldsymbol{e}_x \rightarrow |(\boldsymbol{x}^{(1)} - \boldsymbol{x}^{(2)}) \cdot \boldsymbol{e}_x| - \mathscr{L}$. Of course, the same procedure is repeated for the y and z directions.

We determine the longitudinal and transverse velocity correlations, R_L and R_T respectively, as follows:

$$\left.\begin{aligned} R_L(r) &= \frac{\left\langle \left(\boldsymbol{v}^{(1)}\cdot\boldsymbol{r}_{12}\right)\left(\boldsymbol{v}^{(2)}\cdot\boldsymbol{r}_{12}\right)\middle| |\boldsymbol{r}_{12}| = r\right\rangle_{12}}{\frac{1}{3}r^2\langle \boldsymbol{v}\cdot\boldsymbol{v}\rangle}, \\ R_T(r) &= \frac{\left\langle \left((\boldsymbol{r}_{12}\times\boldsymbol{v}^{(1)})\times\boldsymbol{r}_{12}\right)\cdot\left((\boldsymbol{r}_{12}\times\boldsymbol{v}^{(2)})\times\boldsymbol{r}_{12}\right)\middle| |\boldsymbol{r}_{12}| = r\right\rangle_{12}}{\frac{2}{3}r^4\langle \boldsymbol{v}\cdot\boldsymbol{v}\rangle}, \\ R_T(r) &= \frac{\left\langle \left(\boldsymbol{v}^{(1)}\cdot\boldsymbol{v}^{(2)}\right)\middle| |\boldsymbol{r}_{12}| = r\right\rangle_{12}}{\frac{2}{3}\langle \boldsymbol{v}\cdot\boldsymbol{v}\rangle} - \frac{1}{2}R_L(r). \end{aligned}\right\} \tag{4.9}$$

It is noted that the values of R_L and R_T are normalized in such a way that they would become 1 as $r \downarrow 0$ if they were calculated for fluid particles in a homogeneous and isotropic flow.

In figure 18, results are shown for R_L and R_T as a function of the inter-particle distance r, for three different Stokes numbers: $St = 0.1$, $St = 1$ and $St = 10$. For a relatively small Stokes number such as $St = 0.1$, both the longitudinal and the transversal velocity correlations are close to unity as $r \downarrow 0$. This can be explained by the fact that the particles have relatively little inertia, so that the velocities of two neighbouring particles are almost the same. As r becomes larger, R_L and R_T decrease and eventually they approach zero as $r \to \infty$, as expected. For a larger Stokes number, such as $St = 1$, the particle inertia becomes more important which is reflected by deviations of R_L and R_T from unity for small separation distances. If the particles have a very large Stokes number like $St = 10$, then the velocities of two particles become to a large extent uncorrelated, even if the particles are close together in physical space. Therefore, both R_L and R_T are considerably lower than unity when $r \downarrow 0$. The typical decorrelation length, however, is not altered conceivably with respect to the cases of the lower Stokes numbers.

The RUM component, i.e. the random uncorrelated component of the kinetic energy of the particles, is defined as 1 minus the velocity correlation in the limit that particles are infinitesimally close together:

$$\mathrm{RUM} \equiv 1 - \lim_{r\downarrow 0}\left\langle \frac{\boldsymbol{v}^{(1)}\cdot\boldsymbol{v}^{(2)}}{|\boldsymbol{v}^{(1)}||\boldsymbol{v}^{(2)}|}\middle| |\boldsymbol{r}_{12}| = r\right\rangle_{12}. \tag{4.10}$$

In figure 19, we show the RUM-component of the particle pair velocity as a function of St. The value of RUM is approximately zero for small Stokes numbers, and it increases monotonically with the Stokes number, indicating that the velocities of inertial particles are more and more decorrelated. Eventually, RUM $\to 1$ for sufficiently large Stokes numbers, i.e. the velocities of these particles are entirely decorrelated, even when they are very close to each other.

The RUM component is non-zero for particles with, for example, $St \simeq 0.5$, although the long-time value of $\langle \nabla\cdot\boldsymbol{v}\rangle$ is clearly negative (see figure 15). Thus, the particle segregation may go on indefinitely despite the fact that RUM is present. This contradicts the claim made by Février *et al.* (2005) that RUM is responsible for a saturation of the segregation process.

The results presented in this section show that particle inertia can have major implications for the collision rates between particles. Two effects enhance the collision

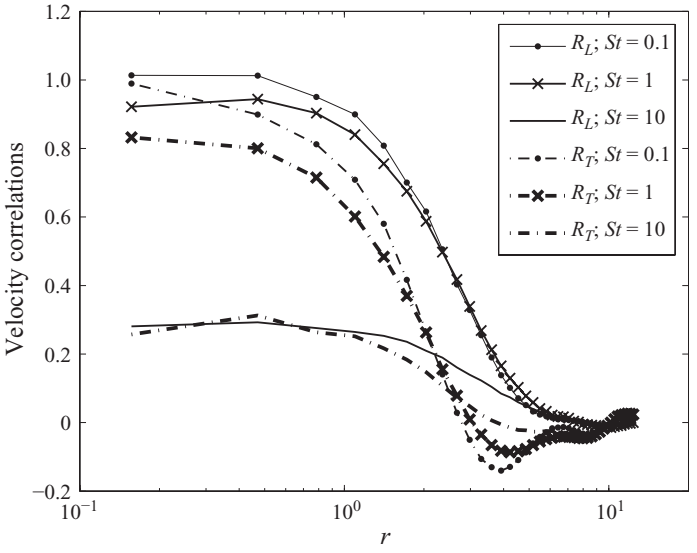

FIGURE 18. Two-particle velocity correlation in longitudinal (R_L) and transversal (R_T) direction as a function of the inter-particle separation distance r in the flow field composed of random Fourier modes, for three different values of the Stokes number.

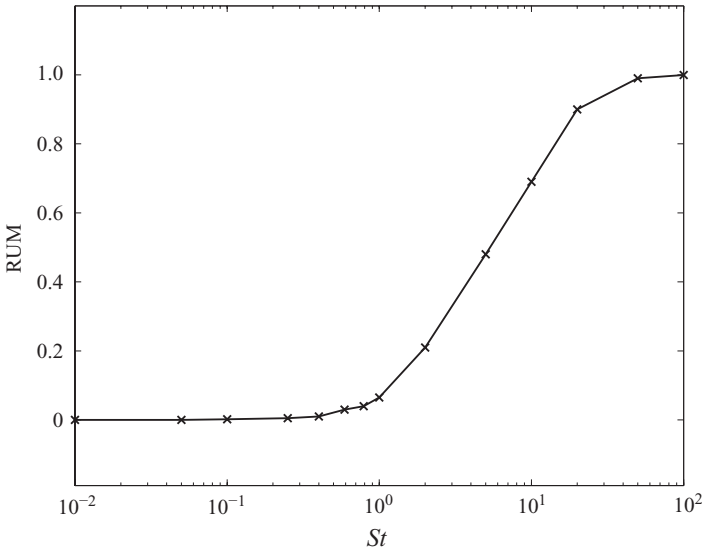

FIGURE 19. RUM component as a function of the Stokes number in the flow field composed of random Fourier modes.

rate between particles: (i) preferential concentration of particles in relatively few regions of the flow, (ii) RUM, i.e. the decorrelation of velocities between neighbouring particles so that particles are more likely to hit each other. From figure 15(a), we know that preferential concentration manifests itself especially for $0.1 < St < 1$. The effect of RUM is most visible for $St > 0.5$ and increasingly important for larger St. Collision rates are therefore expected to be highest in the Stokes number regime $St > 0.5$. Certainly more research is needed to confirm this statement, but the results presented in the seminal paper by Sundaram & Collins (1997) do point in that

direction, since they found a maximum collision rate for a Stokes number St_k (based on the smallest scale of the flow, the Kolmogorov time scale) of $2 < St_k < 5$, with a collision rate vanishing for $St_k \downarrow 0$, and a collision rate decreasing only slowly with St_k if $St_k > 5$.

4.4. *Radial distribution function and process of segregation*

In this section we compare the results for the rate-of-compression presented in § 4.1 and for RUM in § 4.3 with more traditional methods of measuring the particle segregation, in particular the radial distribution function (RDF). The radial distribution function, $g(r)$, gives the number density of particles as a function of the inter-particle distance r (Sundaram & Collins 1997). The total number of particles N_p in a shell between $\hat{r}$ and $\hat{r} + \Delta r$ is

$$N_p\left(\hat{r} - \frac{1}{2}\Delta r < r < \hat{r} + \frac{1}{2}\Delta r\right) = n_0 \int_{\hat{r}-(\Delta r/2)}^{\hat{r}+(\Delta r/2)} 4\pi r^2 g(r)\,\mathrm{d}r, \tag{4.11}$$

where n_0 denotes the particle number density averaged over the entire physical domain, i.e. $n_0 = 10\,000/\mathscr{L}^3$ in our simulations. If all particles are distributed uniformly over the physical domain, then $g(r) = 1$. On the other hand, if particles are preferentially concentrated, on average more particles are found at smaller inter-particles distances, and $g(r) > 1$ for small values of r.

We calculate the RDF by taking into account all particle pairs, and we measure the inter-particle distance $r = |\boldsymbol{r}_{12}|$. Then, the domain in r direction is subdivided into i_{max} bins of size Δr, with r_i the midpoint of the bin. The RDF is then calculated numerically for each r_i, $1 \leqslant i \leqslant i_{max}$:

$$g(r_i) = \frac{N_p\left(r_i - \frac{1}{2}\Delta r < r < r_i + \frac{1}{2}\Delta r\right)}{\frac{4\pi}{3}\left(3r_i^2\Delta r + \frac{1}{4}\Delta r^3\right)n_0}. \tag{4.12}$$

The RDF is plotted in figure 20, for $St = 0.5$ and three different values of i_{max}, after a time $t = 30$. After this time, the radial distribution function has reached a time-converged solution. Apparently, the radial distribution approaches a form $g(r) \propto r^{\beta}$, with $\beta < 0$. It can be shown that β is related to the correlation dimension D_{corr} as follows: $\beta = D_{corr} - 3$ (Bec 2005). Thus, the RDF tends to infinity as $r \downarrow 0$. In order to observe this behaviour in the limit of $r \downarrow 0$, one would need to simulate the motion of an infinite number of particles, measure the RDF for an infinite numbers of bins in the r direction and wait for an infinite time. This is an indication that the segregation process continues indefinitely, which is in agreement with the results presented in § 4.1. Thus, remarkably enough, a time-converged solution of $g(r)$ of the form $g(r) \propto r^{\beta}$ (given a certain finite numbers of bins i_{max}) is in agreement with a segregation process that goes on indefinitely in time.

Finally, we investigate how the RDF depends on the Stokes number. For this purpose, we determine the value of β for a wide range of Stokes numbers, and plot the results in figure 21. Apparently, β is proportional to St^2 if $St \lesssim 0.3$. Comparison with figure 15(b) shows that $\beta \propto \langle \boldsymbol{\nabla} \cdot \boldsymbol{v} \rangle$ in this Stokes number range. For large St, however, the time-converged solution of $\langle \boldsymbol{\nabla} \cdot \boldsymbol{v} \rangle$ becomes positive, while β remains negative. The deviations can be attributed to the presence of RUM, which becomes important for $St \gtrsim 0.5$ (see figure 19). RUM is associated with singularities in the particle velocity field that are not detectable with a box counting method like the

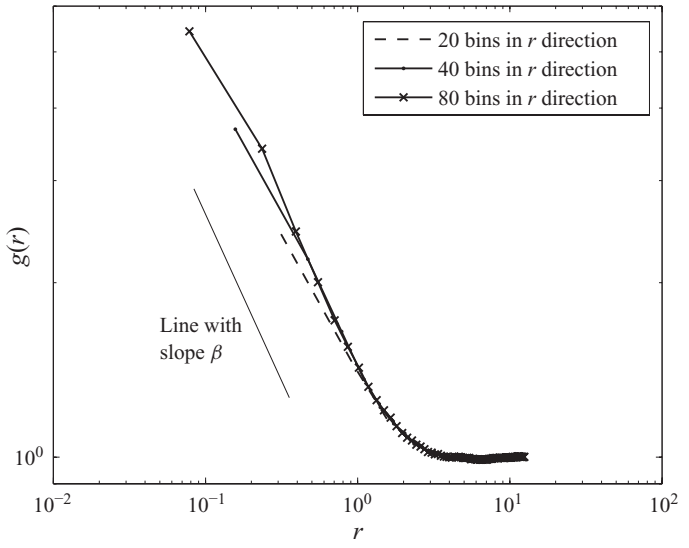

FIGURE 20. Time-converged solution of radial distribution function for three different resolutions in r direction, in the flow field composed of random Fourier modes; $St = 0.5$. In this case, $\beta \simeq -0.65$.

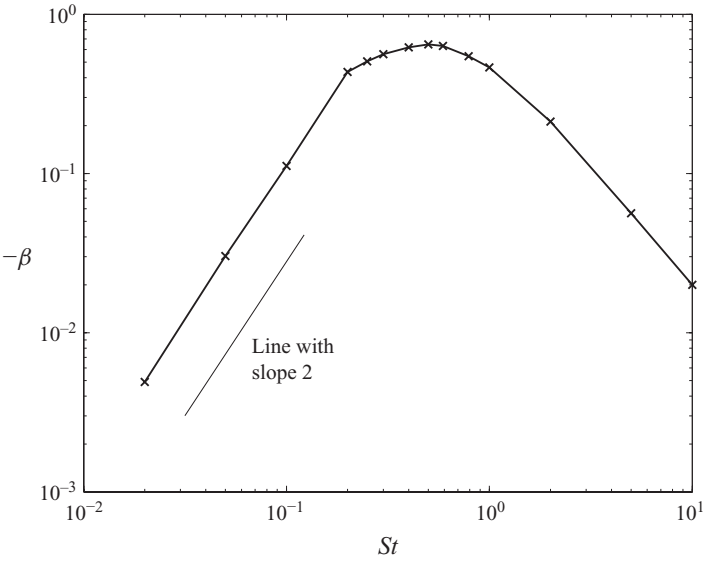

FIGURE 21. Factor β in time-converged solution of radial distribution function with the form $g(r) \propto r^{\beta}$ in the flow field composed of random Fourier modes, as a function of the Stokes number.

RDF. The FLM, however, clearly visualizes the presence of singularities in the particle velocity field and the highly intermittent distribution of particles in turbulent flows.

5. Summary and concluding remarks

We have employed the full Langrangian method (FLM) to study the preferential concentration of inertial particles in turbulent flows. The FLM is based on calculating

the deformation of an initially infinitesimally small volume of particles along the trajectory of one particle. We have demonstrated how this method can be used to determine the compressibility of the particle velocity field, and any spatially averaged moment of the particle number density. The FLM enables the detection of the very high intermittencies in the spatial distribution of particles and the associated singularities in the particle velocity field. These features, which take place on infinitesimally small scales (in the commonly assumed approximation of point particles), can not be identified by box counting methods as they rely on finite box sizes by definition. We have applied the FLM to particle motion in two different random flows: a random straining flow field consisting of counter-rotating vortices and a flow field composed of 200 random Fourier modes. All variables have been made dimensionless on the basis of the mean kinetic energy in the flow and the typical length scale of the flow, allowing a meaningful comparison between the two flow fields.

In the random straining flow, the particle-averaged compressibility of the particle phase is shown to approach a constant value in the course of time. Our results demonstrate that the segregation of particles continues indefinitely if the particle relaxation time is below a threshold value $St_{cr} \sim 2.0$. The long-time limit of the compressibility of the particle velocity field is shown to be approximately linear in the Stokes number for sufficiently small Stokes numbers; this is in accordance with an analytical estimate presented in this paper. The result is valid for an anisotropic flow field consisting of one length scale only, and also for an isotropic flow in which the length scale is varied randomly in time. We show that the probabilility density function of $\nabla \cdot \boldsymbol{v}$ may be very non-symmetric with high intermittent tails. The component of RUM is shown to increase monotonically with the Stokes number. We show that RUM is non-zero even if $St < St_{cr}$, i.e. when particle the particle velocity field is compressed. This means that RUM is present even though the segregation does not stabilize.

The flow field composed of random Fourier modes is an example of a smoothly varying flow field in time and space which mimicks many features of real turbulence such as the presence of regions of non-zero vorticity and non-zero strain. In this flow field, qualitatively the same features are observed as in the random strain flow: the volume occupied by the particle phase decreases continuously if $St < St_{cr}$, with $St_{cr} \sim 0.7$, indicating that the ongoing process of segregation is not limited to relatively simple flow fields. We show analytically that the long-time limit of $\langle \nabla \cdot \boldsymbol{v} \rangle$ is proportional to St^2 for sufficiently small values of St. The higher-order moments of the particle number density are exponentially proportional to time, the factor of proportionality scaling again with St^2. Our results are fully consistent with the theoretical analysis of Balkovsky *et al.* (2001) and with the observation by Chun *et al.* (2005) that the radial distribution function (RDF) approaches the form $g(r) \sim r^{\beta}$ with $\beta < 0$ and $\beta \propto St^2$ for sufficiently small St. RUM becomes important if $St \gtrsim 0.5$; for sufficiently large Stokes number, RUM $\rightarrow 1$, indicating that the particle velocities become virtually uncorrelated with the underlying carrier flow field. The presence of RUM is also visible in the spatially averaged higher-order moments of the particle number density, which show that the particle distrubution may be highly intermittent.

In principle, the FLM is applicable to flows that are unsteady, compressible and/or inhomogeneous, but in the present paper we have restricted the study to incompressible homogeneous turbulence-like flows. Our choice was driven by the need to gain a better understanding and insight into the behaviour of real flows. By using kinematic simulations, we have been able to explore various features such as

compressibility, singularities and RUM as single or related effects and consider their dependence on particle Stokes number and scale in great depth and refinement (see e.g. figures 8, 15 and 17). These studies are an essential preliminary to the application of the FLM to real turbulent flows. For instance, the use of compressibility as a random variable is an important outcome of this work. In order to test the validity of the present model in real turbulence, it is recommended to study the statistics of the rate-of-deformation and RUM also in direct numerical simulations of turbulence.

Appendix. Determination of random coefficients $\boldsymbol{k}^{(n)}$, $\boldsymbol{a}^{(n)}$ and $\boldsymbol{b}^{(n)}$

In this appendix, we describe how the random wavenumbers $\boldsymbol{k}^{(n)}$ and the random coefficients $\boldsymbol{a}^{(n)}$ and $\boldsymbol{b}^{(n)}$ in (2.12) are determined. The coefficients are chosen in such a way that (i) the resulting flow field is periodic in a bounded domain of size $\mathscr{L}\times\mathscr{L}\times\mathscr{L}$, and (ii) the flow approximately satisfies a prescribed energy spectrum $E(k)$.

In order to satisfy periodicity, we know that $\boldsymbol{k}^{(n)}$ must have the form given in (2.13), with $m_1^{(n)}$, $m_2^{(n)}$ and $m_3^{(n)}$ integer numbers. Ideally, $m_1^{(n)2}+m_2^{(n)2}+m_3^{(n)2}=M_{id}^{(n)2}$, where $M_{id}^{(n)2}\equiv k_{id}^{(n)2}\mathscr{L}^2/4\pi^2$, so that the obtained $k^{(n)}=k_{id}^{(n)}$. In the present case $M_{id}^{(n)}$ varies from 1.01 (for $n=1$) to 34.0 (for $n=N$). For each n we pick a random number from a uniform distribution on $\wp[-M_{id}, M_{id}]$ (note that the superscript (n) is dropped for convenience), and we take the integer part of this number in order to obtain $\tilde{m}_1$. Then, we pick a new random number from a uniform distribution on $\wp[-(M_{id}^2-\tilde{m}_1^2)^{1/2}, (M_{id}^2-\tilde{m}_1^2)^{1/2}]$, and take the integer part of it to obtain $\tilde{m}_2^{(n)}$. Finally, the integer number $\tilde{m}_3$ is chosen such that $|M_{id}^2-\tilde{m}_1^2-\tilde{m}_2^2-\tilde{m}_3^2|$ is minimized; the sign of $\tilde{m}_3$ is chosen randomly with equal probability. We redistribute the numbers $\tilde{m}_1$, $\tilde{m}_2$ and $\tilde{m}_3$ randomly with equal probability over the three directions in order to obtain the numbers $m_1^{(n)}$, $m_2^{(n)}$ and $m_3^{(n)}$ as used in (2.13). This procedure is repeated for all N modes.

The random coefficients $\boldsymbol{a}^{(n)}$ and $\boldsymbol{b}^{(n)}$ in (2.12) are determined as follows. First, we pick the length of $\boldsymbol{a}^{(n)}$ and $\boldsymbol{b}^{(n)}$ independently from a Gaussian distribution with mean zero and variance $9/2N$, by using a standard numerical algorithm from Press *et al.* (1992) (Chapter B7). Subsequently, we determine the random direction of $\boldsymbol{a}^{(n)}$ and $\boldsymbol{b}^{(n)}$ in three dimensions by picking three different random numbers, say ξ_1, ξ_2 and ξ_3, from a uniform distribution $\wp[-1, 1]$. If $\rho^2\equiv\xi_1^2+\xi_2^2+\xi_3^2\leqslant 1$, the desired random direction is given by the unit vector $(\xi_1/\rho, \xi_2/\rho, \xi_3/\rho)^T$. If $\rho^2>1$, we pick a new set of three random numbers and repeat doing this until $\rho^2\leqslant 1$. It is noted that the same procedure is equally applicable for determining a random direction in a d-dimensional space by choosing d random numbers $\xi_1, \xi_2, \ldots, \xi_d$.

REFERENCES

Balkovsky, E., Falkovich, G. & Fouxon, A. 2001 Intermittent distribution of inertial particles in turbulent flows. *Phys. Rev. Lett.* **86**, 2790–2793.

Bec, J. 2005 Multifractal concentrations of inertial particles in smooth random flow. *J. Fluid Mech.* **528**, 255–277.

Bec, J., Biferale, L., Cencini, M., Lanotte, A., Musacchio, S. & Toschi, F. 2007 Heavy particle concentration in turbulence at dissipative and inertial scales. *Phys. Rev. Lett.* **98**, 084502.

Chen, L., Goto, S. & Vassilicos, J. C. 2006 Turbulent clustering of stagnation points and inertial particles. *J. Fluid Mech.* **553**, 143–154.

Chong, M. S., Perry, A. E. & Cantwell, B. J. 1990 A general classification of three-dimensional flow fields. *Phys. Fluids* **2** (5), 756–777.

Chun, J., Koch, D. L., Rani, S. L., Ahluwalia, A. & Collins, L. R. 2005 Clustering of aerosol particles in isotropic turbulence. *J. Fluid Mech.* **536**, 219–251.

Crowe, C. T., Chung, J. N. & Troutt, T. R. 1993 Particle dispersion by organized turbulent structures. In *Particulate Two-Phase Flow* (ed. M. C. Roco), vol. 626, chap. 18, p. 1. Heinemann.

Elperin, T., Kleeorin, N. & Rogashevskii, I. 1996 Turbulent thermal diffusion of small inertial particles. *Phys. Rev. Lett.* **76** (2), 224–227.

Falkovich, G., Fouxon, A. S. & Stepanov, M. G. 2002 Acceleration of rain initiation by cloud turbulence. *Nature* **419**, 151–154.

Falkovich, G. & Pumir, A. 2004 Intermittent distribution of heavy particles in a turbulent flow. *Phys. Fluids* **16** (7), L47–L50.

Falkovich, G. & Pumir, A. 2007 Sling effect in collisions of water droplets in turbulent clouds. *J. Atmos. Sci.* **64**, 4497–4505.

Fessler, J. R., Kulick, J. D. & Eaton, J. K. 1994 Preferential concentration of heavy particles in a turbulent channel flow. *Phys. Fluids* **6** (11), 3742–3749.

Février, P., Simonin, O. & Squires, K. D. 2005 Partitioning of particle velocities in gas–solid turbulent flows into a continuous field and a spatially uncorrelated random distribution; theoretical formalism and numerical study. *J. Fluid Mech.* **553**, 1–46.

Frisch, U. 1995 *Turbulence: The Legacy of A. N. Kolmogorov*. Cambridge University Press.

Fung, J. C. H., Hunt, J. C. R., Malik, N. A. & Perkins, R. J. 1992 Kinematic simulation of homogeneous turbulence by unsteady random Fourier modes. *J. Fluid Mech.* **230**, 281–318.

Healy, D. P. & Young, J. B. 2005 Full Lagrangian methods for calculating particle concentration fields in dilute gas–particle flows. *Proc. R. Soc. Lond.* A*:* **461**, 2197–2225.

Hentschel, H. G. E. & Procaccia, I. 1983 The infinite number of generalized dimensions of fractals and strange attractors. *Physica* D **8**, 435–444.

Hunt, J. C. R., Buell, J. C. & Wray, A. A. 1987 Big whorls carry little whorls. *Tech. Rep.* CTR–S87. NASA.

IJzermans, R. H. A. 2007 Dynamics of dispersed heavy particles in swirling flow. PhD thesis, University of Twente, The Netherlands.

IJzermans, R. H. A., Hagmeijer, R. & van Langen, P. J. 2007 Accumulation of heavy particles around a helical vortex filament. *Phys. Fluids* **19**, 107102.

Kraichnan, R. H. 1970 Diffusion by a random velocity field. *Phys. Fluids* **13**, 22–31.

Luo, K., Fan, J. & Cen, K. 2007 Pressure-correlated dispersion of inertial particles in free shear flows. *Phys. Rev.* E **75**, 046309.

Marcu, B., Meiburg, E. & Newton, P. K. 1995 Dynamics of heavy particles in a Burgers vortex. *Phys. Fluids* **7** (2), 400–410.

Maxey, M. R. 1987 The gravitational settling of aerosol particles in homogeneous turbulence and random flow fields. *J. Fluid Mech.* **174**, 441–465.

Maxey, M. R. & Riley, J. J. 1983 Equation of motion for a small rigid sphere in a non-uniform flow. *Phys. Fluids* **26** (4), 883–889.

Osiptsov, A. N. 2000 Lagrangian modelling of dust admixture in gas flows. *Astrophys. Space Sci.* **274**, 377–386.

Ott, E. 1994 *Chaos in Dynamical Systems*. Cambridge University Press.

Press, W. C., Flannery, B. P., Tucholsky, S. A. & Vetterling, W. T. 1992 *Numerical Recipes in Fortran 77*. Cambridge University Press.

Reeks, M. W. 1977 On the dispersion of small particles suspended in an isotropic turbulent fluid. *J. Fluid Mech.* **83** (3), 529–546.

Reeks, M. W. 2004 Simulation of particle diffusion, segregation, and intermittency in turbulent flows. In *Proc. IUTAM Symposium on Computational Modelling of Disperse Multiphase Flow* (ed. S. Balachandar & A. Prosperetti), pp. 21–30. Elsevier.

Shaw, R. A. 2003 Particle-turbulence interactions in atmospheric clouds. *Annu. Rev. Fluid Mech.* **35**, 183–227.

Sommerer, J. C. & Ott, E. 1993 Particles floating on a moving fluid: a dynamically comprehensible physical fractal. *Science* **259**, 335–339.

Spelt, P. D. M. & Biesheuvel, A. 1997 On the motion of gas bubbles in homogeneous isotropic turbulence. *J. Fluid Mech.* **336**, 221–244.

Squires, K. D. & Eaton, J. K. 1991 Measurements of particle dispersion obtained from direct numerical simulations of isotropic turbulence. *J. Fluid Mech.* **226**, 1–35.

Sundaram, S. & Collins, L. R. 1997 Collision statistics in an isotropic particle-laden turbulent suspension. Part 1. Direct numerical simulations. *J. Fluid Mech.* **335**, 75–109.

Wang, L. P. & Maxey, M. R. 1993 Settling velocity and concentration distribution of heavy particles in homogeneous isotropic turbulence. *J. Fluid Mech.* **256**, 27–68.

Wang, L. P., Wexler, A. S. & Zhou, Y. 1998 On the collision rate of small particles in isotropic turbulence. II. Finite inertia case. *Phys. Fluids* **10** (10), 1206–1216.

Wilkinson, M., Mehlig, B., Östlund, S. & Duncan, K. P. 2007 Unmixing in random flows. *Phys. Fluids* **19**, 113303.

Zaichik, L. I. & Alipchenkov, V. M. 2003 Pair dispersion and preferential concentration of particles in isotropic turbulence. *Phys. Fluids* **15** (6), 1776–1787.